Developmental Biology 390 (2014) 191–207

Contents lists available at ScienceDirect

Developmental Biology

journal homepage: www.elsevier.com/locate/developmentalbiology

AcvR1-mediated BMP signaling in second heart field is required for arterial pole development: Implications for myocardial differentiation and regional identity

Penny S. Thomas, Sudha Rajderkar, Jamie Lane, Yuji Mishina, Vesa Kaartinen *

Department of Biologic and Materials Sciences, University of Michigan – Ann Arbor, 1011 N. University Ave, Ann Arbor, MI 48109, USA

ARTICLE INFO

Article history:
Received 13 January 2014
Received in revised form
17 March 2014
Accepted 18 March 2014
Available online 27 March 2014

Keywords:
Cardiac development
Second heart field
Conotruncal defects
BMP signaling
Receptors

ABSTRACT

BMP signaling plays an essential role in second heart field-derived heart and arterial trunk development, including myocardial differentiation, right ventricular growth, and interventricular, outflow tract and aortico-pulmonary septation. It is mediated by a number of different BMP ligands, and receptors, many of which are present simultaneously. The mechanisms by which they regulate morphogenetic events and degree of redundancy amongst them have still to be elucidated. We therefore assessed the role of BMP Type I receptor AcvR1 in anterior second heart field-derived cell development, and compared it with that of BmpR1a.

By removing *Acvr1* using the driver *Mef2c[AHF]-Cre*, we show that AcvR1 plays an essential role in arterial pole morphogenesis, identifying defects in outflow tract wall and cushion morphology that preceded a spectrum of septation defects from double outlet right ventricle to common arterial trunk in mutants. Its absence caused dysregulation in gene expression important for myocardial differentiation (*Isl1*, *Fgf8*) and regional identity (*Tbx2*, *Tbx3*, *Tbx20*, *Tgfb2*). Although these defects resemble to some degree those in the equivalent *Bmpr1a* mutant, a novel gene knock-in model in which *Bmpr1a* was expressed in the *Acvr1* locus only partially restored septation in *Acvr1* mutants. These data show that both BmpR1a and AcvR1 are needed for normal heart development, in which they play some non-redundant roles, and refine our understanding of the genetic and morphogenetic processes underlying Bmp-mediated heart development important in human congenital heart disease.

Introduction

Heart morphogenesis is a complex process involving many secreted growth factors and their receptors (reviewed by Bruneau (2013)). Bone morphogenetic protein (BMP)-mediated signaling has been strongly implicated in the process by which separate ventricular outlets, valves and arterial trunks are formed from a single tube by septation requiring precise shape and positioning of contributory structures (reviewed by Dyer and Kirby (2009)). Failure in this process results in formation of outflow tract (OFT) septation defects, one of the common cardiac birth defects in humans.

The arterial pole of the developing heart is largely composed of mesodermally-derived second heart field (SHF), which forms myocardium of the interventricular septum and right ventricle (RV), and myocardium and future smooth muscle (arterial trunk) of the OFT wall. It also contributes to the adjacent endocardium, and cushion mesenchyme, especially proximally, by endocardial-to-mesenchymal transformation (EMT). The mesenchyme of OFT cushions is largely composed of cardiac neural crest-derived cells (CNCC), which also contribute to arterial trunk smooth muscle (Dyer and Kirby, 2009; Snarr et al., 2008; Verzi et al., 2005).

BMPs have been shown to exert complex, dose-dependent and even opposing effects on myocardial differentiation, functioning as both promoters and inhibitors of cardiac growth (de Pater et al., 2012). It has been suggested that a delicate balance between FGF and BMP signaling controls proliferation and differentiation of SHF progenitors (Hutson et al., 2010) and that BMPs can block FGF signaling (Tirosh-Finkel et al., 2010). In mouse embryos, inactivation of genes encoding BMPs 2,4 and 7 or BmpR1a (Bone morphogenetic protein receptor, type Ia) specifically in the second heart field has been shown to result in formation of common arterial trunk and OFT cushion defects (Bai et al., 2013; Briggs et al., 2013; Wang et al., 2010; Yang et al., 2006). BMPs have also been shown to regulate myocardial differentiation through a microRNA-mediated mechanism, and *Bmpr1a* needed for expression of

* Corresponding author. Fax: +1 734 647 2110.
E-mail address: vesak@umich.edu (V. Kaartinen).

http://dx.doi.org/10.1016/j.ydbio.2014.03.008
0012-1606/

T-box transcription factors *Tbx2* and *Tbx3*. These are important for myocardial differentiation and arterial pole morphogenesis (Mesbah et al., 2012; Singh et al., 2012).

BMPs signal via tetrameric transmembrane receptor complexes composed of two Type II (BmpRII, AcvRIIa or AcvRIIb) and two Type I (BmpRIa [Alk3], BmpRIb [Alk6] or AcvRI [Alk2; Activin A receptor, type Is]) receptors (Massague and Chen, 2000). Ligand binding results in activation of Type I receptor kinase activity, which subsequently phosphorylates receptor-regulated R-Smads 1,5 or 8 (Derynck and Zhang, 2003). Phosphorylated R-Smads and Smad4 form a complex which accumulates in the nucleus where it functions as a transcriptional co-regulator. Evidence suggests there is a limited degree of redundancy between BMP receptors underlying regulation of developmental events (Kishigami and Mishina, 2005). The situation is complex; heteromeric as well as homomeric ligand dimers can bind with different binding affinities to oligomeric receptor complexes composed of different type II and type I and co-receptors (Ehrlich et al., 2012), at least in model systems.

Although an essential role for BmpRIa has been demonstrated, it is not the only type I receptor expressed in the heart. AcvRI has been shown to play critical roles in endocardial cushion and OFT valve development in mice (Kaartinen et al., 2004; Thomas et al., 2012; Wang et al., 2005) and mutations in *ACVR1* have been implicated in congenital cardiac defects in humans (Smith et al., 2009). We therefore chose to investigate the role of AcvRI specifically in the second heart field and its derivatives.

Materials and methods

Mice

Mice carrying the conditional *Acvr1-flox* allele ($Acvr1^{F}$), *Bmpr1a-flox* allele ($Bmpr1a^{F}$), 'constitutively active' *Acvr1* conditional allele (*ACVR1* carrying Q207D mutation, '*caAcvr1*') and *Mef2c[AHF]-Cre* transgenic mice (kindly provided by BL Black) were used and genotyped as previously described (Ahn et al., 2001; Fukuda et al., 2006; Kaartinen and Nagy, 2001; Verzi et al., 2005). Timed matings between $Acvr1^{KO/WT}$ *Mef2c[AHF]-Cre*$^{+}$ males and $Acvr1^{F/F}$ female mice were used to obtain $Alk2^{F/KO}$*Mef2c[AHF]-Cre*$^{+}$ tissue-specific mutant embryos ('*Acvr1-cKO*'). Some females were also $R26R^{YFP/YFP}$ or $R26R^{lacZ/lacZ}$ to enable *Mef2c [AHF]-Cre* lineage tracing, and FACS-based isolation of recombined second heart field cells (see below). Controls were either Cre^{0}, or $Acvr1^{F/WT}$, *Mef2c[AHF]-Cre*$^{+}$ littermates ('*Acvr1-cHet*'). To generate other experimental genotypes, females were generated carrying various combinations of *floxed* and wild type alleles of both *Acvr1* and *Bmpr1a*, or with $Acvr1^{Bmpr1a\text{-}KI}$, or $Acvr1^{ACVR1\text{-}KI}$ (see below, and main text), and $Bmpr1^{F/WT}$ *Mef2c[AHF]-Cre*$^{+}$ and $Acvr1^{F/WT}$,$Bmpr1^{F/WT}$, *Mef2c[AHF]-Cre*$^{+}$ males.

Ethics statement

This study was carried out in strict accordance with the recommendations in the Guide for the Care and Use of Laboratory Animals of the National Institutes of Health. The experiments described in this study were specifically approved by the University Committee on Use and Care of Animals of the University of Michigan-Ann Arbor (Protocol Number: #09944).

Generation of $Acvr1^{nlsLacZ}$ bac transgenic mice

A *nlsLacZ-pA* cassette was inserted in frame into the first coding exon of *Acvr1* (exon 3) in the *bac* RP23-366D15 (Children's Hospital Oakland Research Institute) by using standard recombineering techniques (Warming et al., 2005) (see Fig. 5). Bac transgenic mice were generated in the University of Michigan Transgenic Animal Model Core. Three of five founders displayed similar staining patterns consistent with authentic *Acvr1* expression (data not show). The line #934 was used for further studies.

Generation of $Acvr1^{Bmpr1a\text{-}Flag}$ (Bmpr1a-KI) and $Acvr1^{ACVR1\text{-}His6Myc}$ (ACVR1-KI) knockin mice

The coding region of the *Bmpr1a* cDNA (from ATCC) was subcloned into pcDNA3.1 vector (Invitrogen), and sequences encoding the Flag-tag inserted in frame into the 3′end of the cDNA by site-directed mutagenesis (QuikChange II XL; Agilent). A similar strategy was used to modify human *ACVR1A* cDNA (kindly provided by R. Derynck) by inserting sequences encoding the His6/Myc-tag into its 3′end. Targeting vectors were generated as follows: a long 5′ homology arm covering a 5-kb segment of the mouse genomic DNA upstream of the *Acvr1* translational start in exon 3 and a short 3′ homology arm covering a 2.6-kb segment of DNA downstream of the exon 3/intron 3 boundary were PCR-amplified using the mouse bac DNA as a template, and subcloned into a cloning vector containing the Flag-tagged *Bmpr1a-bGHpolyA* (or Myc-His6-tagged *ACVR1-bGHpolyA*) and the *loxP-PGK-Neo-polyA-loxP* cassettes (*DTA* was used a negative selection marker) (see Fig. 7). Electroporation, screening, validation, removal of the selection marker, ES cell expansion, blastocyst injections and production of chimeric and heterozygote mice were performed according to standard procedures by genOway (France).

LiCl treatment

Pregnant female mice were injected intraperitoneally with LiCl (200 mg/kg in saline) once a day at E7-E10 (NaCl [200 mg/kg] was used as a control) as described (Tian et al., 2010).

Histology, immunohistochemistry and in situ hybridization

Embryos for assessment were collected in sterile DBPS and fixed overnight in commercial 10% formalin or fresh 4% paraformaldehyde in PBS at 4 °C overnight. Those for wax embedding were then washed, dehydrated, and oriented and embedded in fresh Blue Ribbon Tissue Embedding/Infiltration Medium (Leica Surgipath) after three changes. 7 μm sections were cut and mounted on Superfrost plus slides (Fisher) and stored at room temperature or 4 °C. Haematoxylin and eosin staining was performed using a standard protocol, taking care to ensure complete, but not over-, staining to allow maximum discrimination of cell types. **Immunohistochemistry (see Supplemental Table 1 for details)** performed on rehydrated wax sections: Antigen retrieval (15 min at 95–100 °C) in citrate buffer pH6 was used in some cases, tissues blocked with 2–3% BSA, 0.1% Triton-X100 in PBS or TBS prior to incubation with primary antibodies overnight at 4 °C. Binding was visualized with Alexafluor-594 or -488-conjugated secondary antibodies (Life Technologies) on slides mounted with Vectamount/DAPI (Vector Labs).

Some fixed embryos were processed for cryo-embedding: washed in PBS, allowed to sink in sterile 10% sucrose in PBS, then 7% gelatin (Sigma G6650, 75 bloom), 15% sucrose in PBS, oriented and embedded in fresh 7% gelatin, 15% sucrose in PBS on ice then dry ice, and stored at −20 or −80 °C. 10 μm cryo sections were cut and stored at −20 or −80 °C.

Immunohistochemistry performed on cryo sections

Antigen retrieval was not used unless stronger/more complete MF20 or α-SMαA signal was needed. α-GFP detected YFP lineage-tracing but any heat-based antigen retrieval prevented its detection.

For quantification of proportion of pSmad1/5/8-positive cells in OFT column cells, immunofluorescence was performed using α-

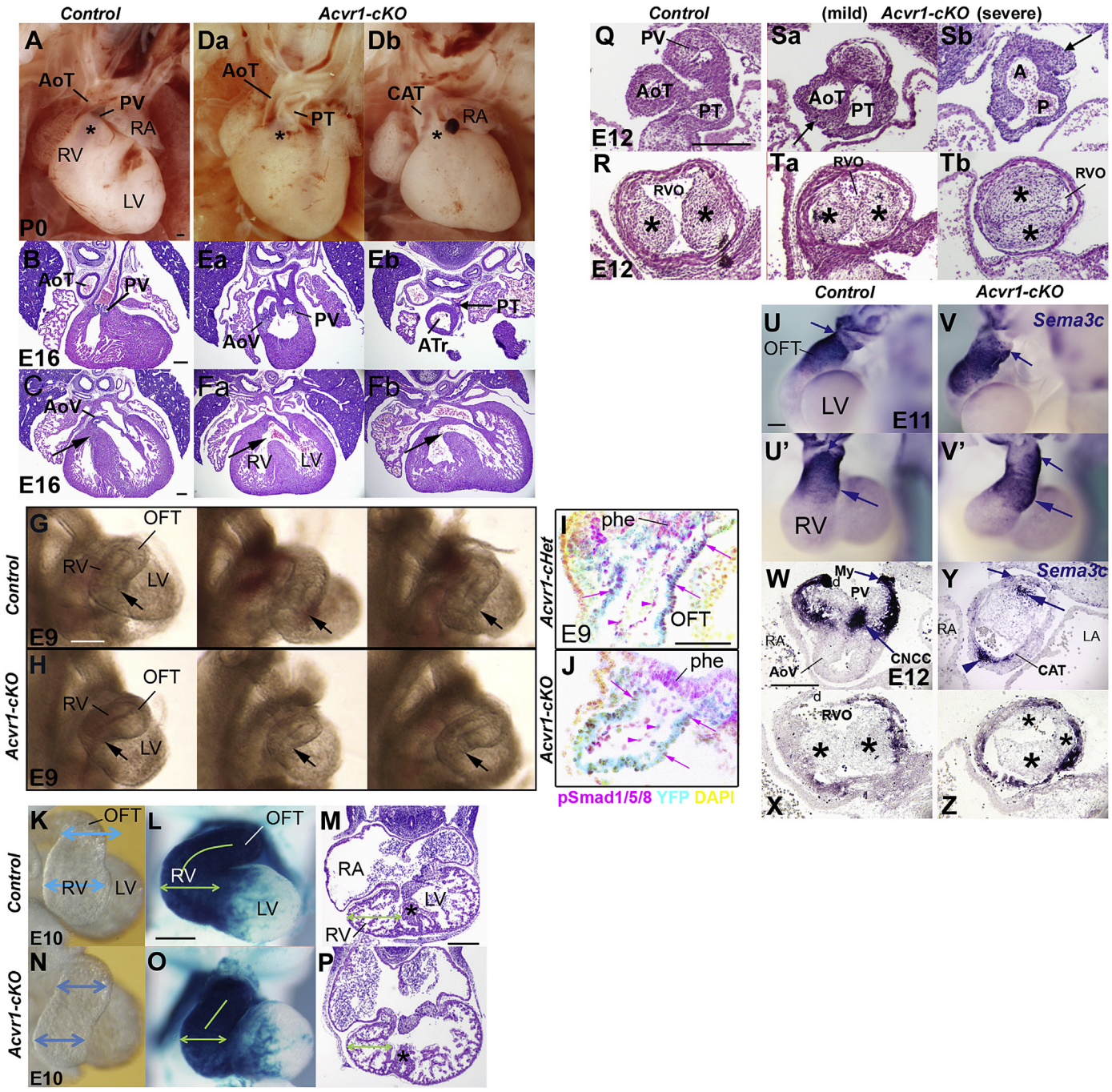

Fig. 1. Abnormal morphology in *Acvr1-cKO* hearts and trunks. A,Da,Db, P0 hearts; B,C,Ea–Fb, E16 4-chamber H&E: Post-septation stage controls (A,B) have aortic and pulmonary trunks at right angles to one another, proximal AoT behind sub-pulmonary sleeve (asterisk in A). In 'mildest' *Acvr1* cKO (Da,Ea,Fa), DORV, trunks parallel to one another, valves on same level as one another, proximal AoT visible (Da) as subpulmonary sleeve inadequate, insufficient displacement of AoT to the left posterior/PT to the right anterior. In 'severe' Acvr1 cKO (Db,Eb,Fb) single trunk close to valve, though often distally septated to form separate full size (not shown) or rudimentary second trunk (PT in Eb connected to pulmonary arteries). DORV (Fa), CAT (Fb) accompanied by subvalvular VSD (black arrow). G,H,E9; I,L, E10; hearts in situ from right: Three representative E9 mutant hearts (H) distinguishable from three controls (G) by variably narrower RV apex (arrow) vs OFT (RV+OFT of these samples used for qRT-PCR, Figs. 3 and 4). I,J, E9 4-chamber cryosections showing less nuclear phosho-Smad1/5/8 immunostaining (pink) in OFT wall (pink arrows) in *Mef2c[AHF]-Cre*-recombined cells (YFP, cyan) in *Acvr1-cKO* (J) than in *Acvr1-cHet* control (I). Endocardium also positive (arrowheads). Unrecombined endoderm same in both (phe). E10 control RV broader (blue arrows) than OFT (K) unlike mutant (N). L,O, *Mef2c[AHF]-Cre* lineage βgal stain (blue), apical view: control (L) RV is broader laterally (green arrows), proximal OFT curves to reach midline (green line) unlike mutant (O). N,P, E11, 4-chamber,H&E: mutant (P) RV apex grows but remains narrower laterally than in control (N), though wall thickness and trabeculation very similar and muscular septum (asterisk) present (contacts AV cushion in different section from N). Scale bar, 200 μm. **'Rotation' of OFT less in mutant hearts.** Q–Tb, E12 transverse to OFT, H&E: In control (Q), AP septation complete, distal trunks separate, lying in correct relation to one another; proximal to valve cushions, parietal and septal cushions (*) lie parallel to A–P axis (R) so RVO anterior-most. In mild mutant, some partial distal trunk septation (Sa) present only, but main OFT cushions (*) near correct orientation (Ta); in severe mutant, no distal trunk septation, aortic (A) and pulmonary (P) lumens unseparated (Sb). More proximally (Tb), cushion faces 60° short of normal orientation. *Note* irregular trunk wall (arrow, Sa,Sb). U–Z, *Sema3C* expression, E11, WMT ISH; E12, section ISH: In control E11 (U from left, U′ from anterior) strongest (small arrows) on distal anterior/left face; in mutant (V from left, V′ from anterior) strongest distal left to posterior, less cleanly defined. Expression extends more proximally in mutant (large arrow). Control E12, valve level (W), strongest myocardial (My) expression on anterior face (RVO) (tissue split anteriorly, d) but in mutant (Y in which distal septation failed), very weak on anterior face (small arrow), strong posteriorly (arrowhead); positive NC cells abnormally located (large arrow). Proximally, expression weak in control (X), more extensive in mutant (Z: note abnormal cushion* morphology). d, artifactual damage. Scale bar, 200 μm.

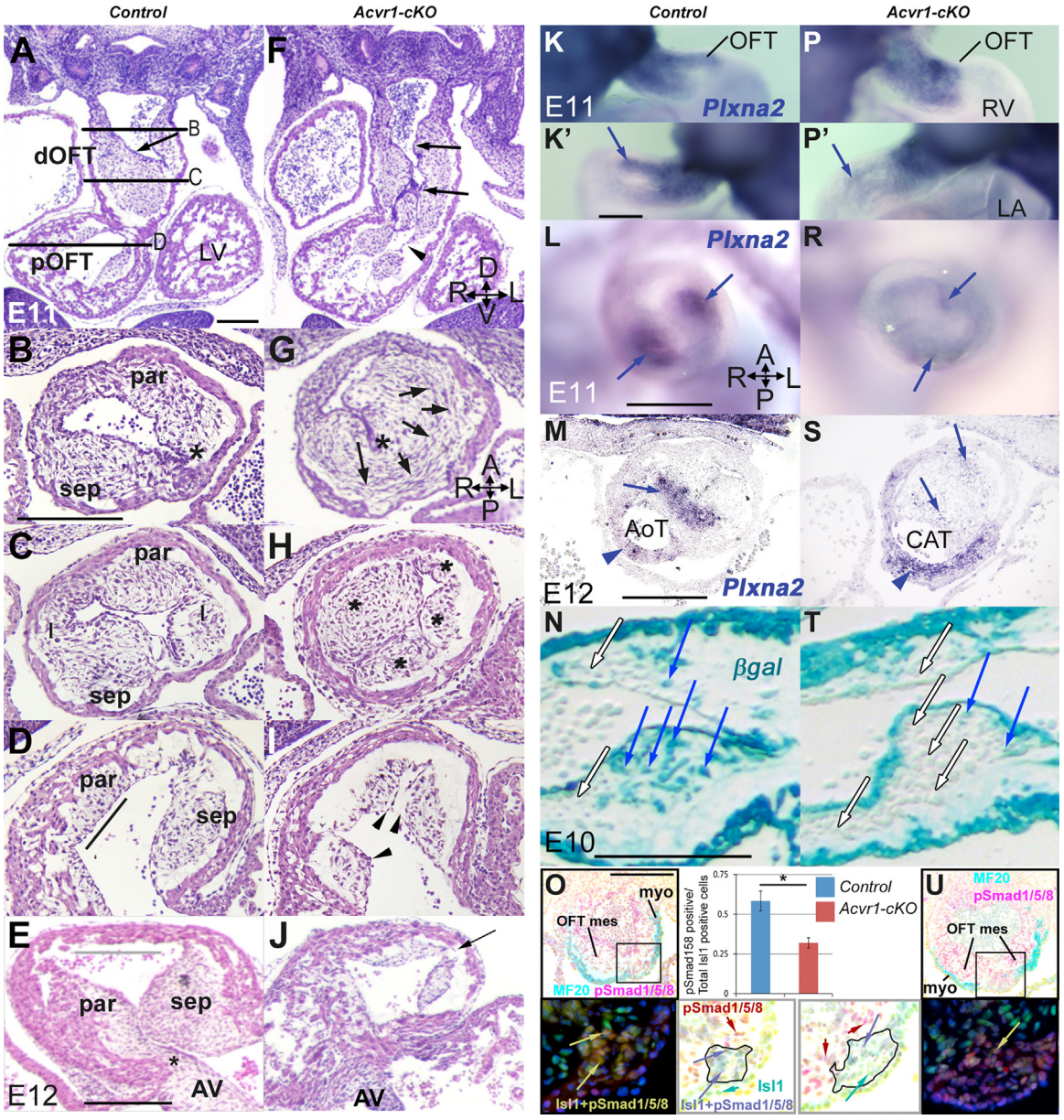

Fig. 2. Abnormalities in OFT cushions in *Acvr1-cKO*. A–J, E11, E12 H&E; B–E,G–J transverse to OFT: Parallel to the distal OFT, endocardial contour (arrow) smooth in control (A) but irregular (arrows) and cushion continuity poor (arrowhead) in mutant (F). Distally, two cushions (par, sep) present in control (B) leave endocardium fairly close to OFT wall (asterisk), but in mutant (G) one large dysmorphic cushion, with circumferentially oriented cells on left side (arrows), create a greater distance to between wall and endocardium (asterisk) and functional lumen remains only in right anterior position. Mid-OFT, four cushions (par, sep, I, I) in control (C), abnormal cushion size and location (asterisks) in mutant (H). Proximal cushions faces are parallel to flow (line) in control (D), but an abnormal pyramidal cushion contour (arrowheads) in mutants (I). By E12, parietal cushion continuity with AV cushion present (asterisk), wide cushion-free RV outlet (line) anteriorly in control (E) but undersized proximal cushions, no continuity with AV cushion, no cushion-free outlet space (arrow) in mutant (J). K–S, E11-12, *Plxna2* ISH: From both right (K,P) and left (K′,P′) *Plxna2*-positive cells present in both control (K,K′) and mutant (P,P′) OFT, though staining mid-OFT in mutant (arrows) weaker. Mid-OFT, strong expression in central cells of each main OFT cushion in control (L), faint misplaced expression in mutant (R). By E12, strong expression in condensed central mesenchyme (arrow) at level of valve septation in control (M), faint in aortic trunk (arrowhead); faint in mutant cushion (S, arrows) but strong expression in irregular thickness arterial wall (arrowhead). N,T, E10, βgal stain, sagittal sections: in *Acvr1-cHet Mef2c[AHF]-Cre* control, numerous recombined mesenchymal cells (blue arrows) underlie recombined endocardium (N) in proximal cushion, but very few in *Acvr1-cKO* (T). Unrecombined mesenchyme (white arrows) and endocardium also present. O,U, E11, transverse distal OFT sections, immunostaining: Upper panels show MF20, α-pSmad1/5/8 immunostaining on sections in which the region including a particular column of SHF-derived cells is indicated by a box (see also Online Fig. 4). Lower panels: darkfield and color-inverted images show an enlargement of the equivalent areas in sister sections to those in the upper panels, demonstrating that the population of Isl1-positive, MF20-negative cells there (outlined in color-inverted images) contained more pSmad1/5/8-positive cells in the control than in the mutant sample (quantification shown in bar chart; $n=4$, $\pm$SEM, $^*p<0.01$). Examples of Isl1-positive, pSmad1/5/8-negative cells (green arrows); Isl1-negative, pSmad1/5/8-positive cells (red arrows); and Isl1-positive/pSmad1/5/8-positive cells (yellow arrows on darkfield, blue arrows on color-inverted image) identified. Note many pSmad1/5/8-positive mesenchymal cells in both control and mutant sections (red cells in color-inverted images). AV, atrioventricular cushion; dOFT, distal OFT; I, intercalated cushion; pOFT, proximal OFT; par, parietal cushion; sep, septal cushion. Embryonic axes in F,G,M: A, anterior; D, dorsal; L, left; P, posterior; R, right; V, ventral. Scale bar, 200 μm.

pSmad1/5/8 and either α-Isl1 or MF20 on 10 μm cryostat sections of E11 control and mutant samples, cut transverse to the OFT. Using single channel gray scale images and combined color images, column cells (positive for Isl1 but negative to MF20) were quantified in each section, and the proportion showing positive α-pSmad1/5/8 staining as assessed by comparison with positive non-recombined cells determined.

For cell proliferation analysis, immunofluorescence was used on 10 μm cryostat sections cut 4-chamber, parallel to OFT, with α-phosphohistone3 (PH3) and either MF20, α-GFP or α-Isl1. Every

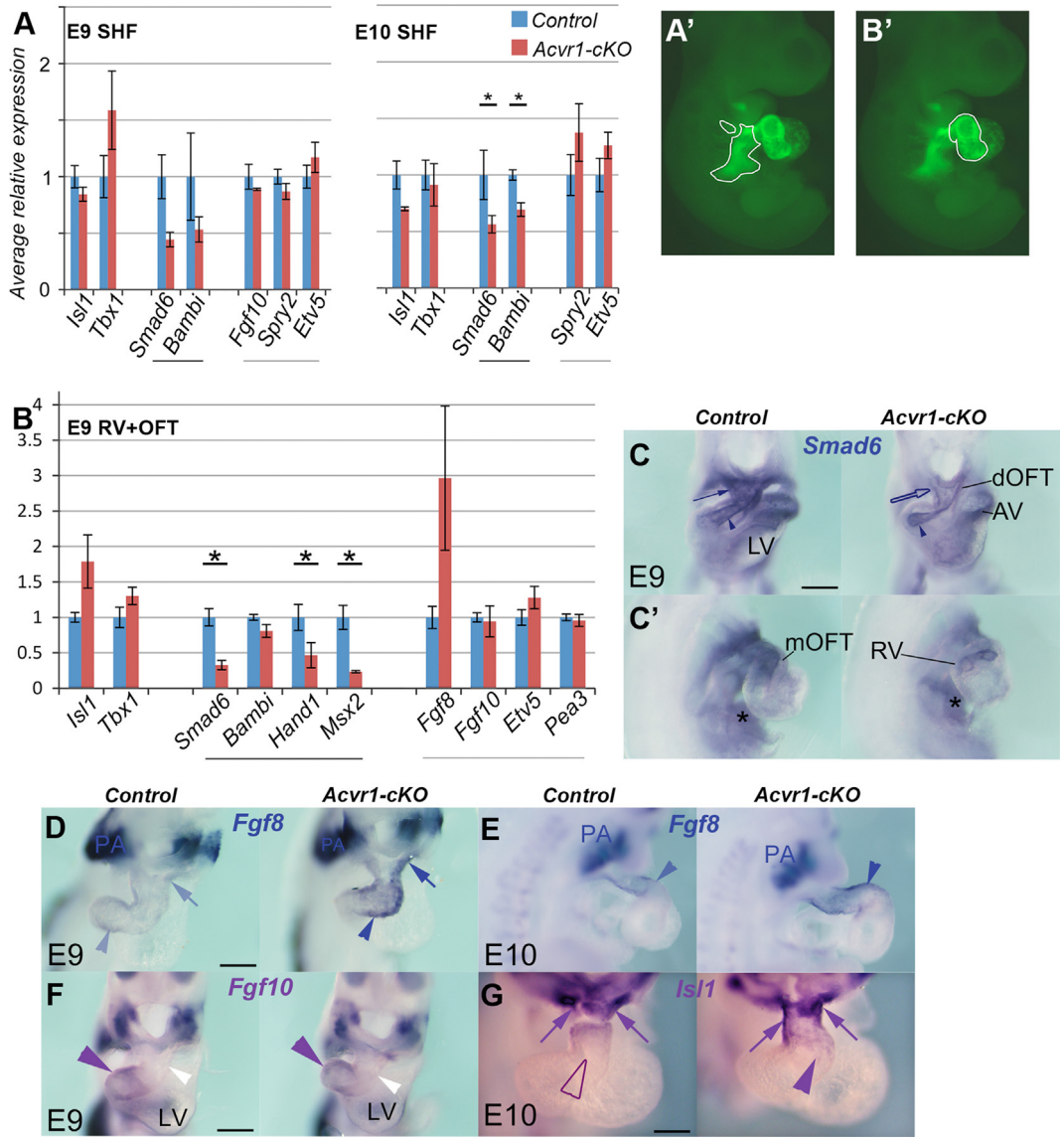

Fig. 3. Gene expression differences between *Acvr1-cKO* and controls (I). A, qRT-PCR, E9 and E10, SHF cells (YFP+ve *Mef2c[AHF]-Cre*-recombined population, outlined in A′ at E9, from right) FACS-sorted after removing the OFT/heart tube. control, blue bars; *Acvr1-cKO*, red bars. Average *Bmp* synexpression gene expression (black underline) reduced in mutants at both time points. *Fgf* synexpression target gene expression (gray underline) slightly elevated at E10. *Tbx1* expression higher at E9, and *Isl1* less at E10 in mutants. Results are average of $n \geq 3$ each control, *Acvr1* cKO samples, $\pm$SEM, $^*p \leq 0.05$. B, qRT-PCR on E9 RV+OFT (manually dissected region, outlined in B′, in YFP+ve *Mef2c[AHF]-Cre*-recombined population). Average BMP target gene expression (black underline) reduced in mutants, *Fgf8* expression much higher, but not *Fgf10* or FGF targets. *Isl1* and *Tbx1* also elevated. C–G, E9, E10 WMT ISH for gene expression reported in B, control on left, mutant on right. C 4-chamber, C′ from right, *Smad6* strong in distal (arrow)-mid OFT and adjacent SHF in control, greatly reduced in mutant (also inner curvature/RAV). Endocardium (arrowhead), LAV and liverbud (asterisk) positive in both. D, *Fgf8* strong distal (arrow) to proximal OFT (arrowhead) in mutant but weak in control; E, *Fgf8* stronger, extends more proximally (arrowhead) in mutant. Endoderm expression strong in all (PA). F, *Fgf10* expression similar in both control and mutant, stronger in proximal/mid OFT (purple arrowhead) than distal (white). G, *Isl1* strong distally (arrows) but also extends to mid-OFT (arrowhead) in mutant. dOFT, mOFT, distal, mid, outflow tract $^*p \leq 0.05$. Scale bar, 200 μm.

α-PH3-positive wall cell was counted that was also within MF20/α-GFP-positive region within the morphologically definable OFT. MF20-negative second heart field cells were not included. Proximal and distal OFT were distinguished by direction of heart tube. Three separate control and mutant samples (19–22 pair somite stage) paired by size were counted and were assessed. **Apoptotic cells** were detected using Dead End Fluorometric TUNEL system (Promega) following manufacturer's instruction.

RNA in situ hybridization

Embryos for ISH were fixed in freshly thawed 4% paraformaldehyde in PBS over night at 4 °C. Those for section ISH were washed and wax-embedded, sectioned at 10 μm and mounted as described above. DIG-labeled RNA probes (see Supplemental Table 2 for details) were made using a DIG-labeled NTP mix (Roche Applied Sciences) according to manufacturer's instructions, stored at −80, or −20 °C diluted in hybridization buffer. Section ISH was performed as described (Moorman et al., 2001) with probes diluted to 1 ng μl^{-1} or less. After staining, sections were washed, fixed and mounted in Immumount (Thermo Scientific).

Embryos for wholemount ISH were fixed as above, washed in PBST, dehydrated and stored in 95% methanol, 5% PBST at −20 °C. After rehydration they were trimmed to enable access of reagents, visualization of OFT or other tissues in cross section without sectioning in some cases, and easy discrimination of controls and mutants (which were then processed together for all steps), proteinase K-treated, post-fixed and pre-hybridized rotating for at least 1 h in standard non-SDS-based hybridization buffer, pH5, at 70 °C. Probe (for final concentration of 0.1–1 ng μl^{-1}) was added, or buffer replaced with pre-heated

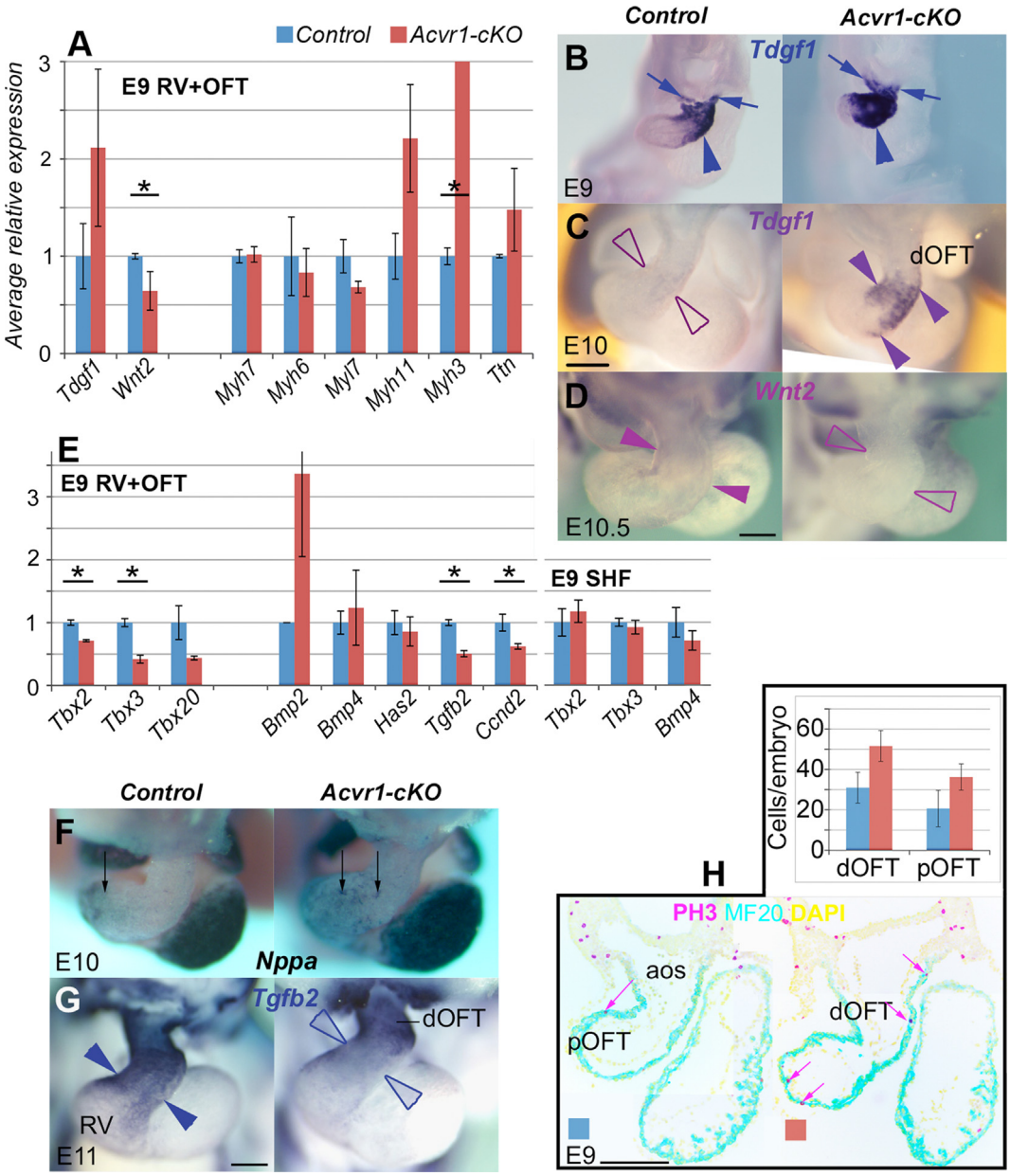

Fig. 4. Gene expression differences between *Acvr1-cKO* and controls (II). A, qRT-PCR on E9 RV+OFT for muscle-related gene expression differentiation (control, blue; mutant, red): Though average expression of sarcomeric protein genes *Myh7*, *Myh6* not affected, *Myl7* lower, *Myh11* and *Myh3* higher (expression levels too low for WMT ISH). *Tdgf1* (*Cripto*) variably higher, *Wnt2* lower in mutants. Results are average of $n \geq 3$ each control, *Acvr1* cKO samples, $\pm$SEM, $^*p \leq 0.05$. B–D E9, E10 WMT ISH for gene expression reported in A, control on the left, mutant on the right: B, *Tdgf1* expressed in OFT distally (arrows) to mid/proximally (arrowhead) more strongly in mutant than control, still detectable E10 (arrowheads) only in mutants. L, *Wnt2* detectable throughout OFT (arrowheads) but not in mutant. E, qRT-PCR on E9 RV+OFT, SHF for average *Bmp/Tbx* regional gene expression, control blue, mutant red: *Tbx2*, *Tbx3*, *Tbx20*, *Tgfb2*, *Ccnd2* all reduced in mutant RV+OFT; *Tbx2*, *3* not affected in mutant SHF; *Has2*, *Bmp4* no difference; *Bmp2* higher in mutant RV+OFT. Results are average of $n \geq 3$ each control, *Acvr1* cKO samples, $\pm$SEM. $^*p \leq 0.05$. F–H, WMT ISH and proliferation related to gene expression reported in E, control on the left, mutant on the right: F, *Nppa* expressed more broadly mid-OFT in mutant (arrows); G, *Tgfb2* much lower mid-proximal OFT (arrowheads) in mutant. H, average proliferation higher in mutant than control MF20 (cyan)-positive OFT wall (α-PH3-labeled nucleus: pink arrow): bar chart ($n=3$ control, mutant) on left, representative sections of control (middle) and mutant (right). aos, aortic sac; dOFT, pOFT distal, proximal outflow tract; PA pharyngeal arch; PH3, phosphohistone 3. $^*p \leq 0.05$. Scale bar, 200 μm.

previously used probe in hyb buffer, and left rolling overnight. Used probe was recovered and stored at −20 °C, but discarded when staining level reduced. Embryos were then washed (rolling) for 20 min three times in pre-heated hybridization buffer at 70 °C, once in hybridization buffer/TBST, then in at least 6 changes of TBST at room temperature over 1 h, blocked in 0.05% Roche block (one hour) and rocked O/N at 4 °C with α-DIG Fab fragments (Roche Applied Sciences,1:2000–5000); washed with 10 changes of TBST the next day (RT), rolling, over several hours, and O/N at 4 °C, stationary if E9 or 10; rolled for 10 min (RT) twice in NTMT pH9.5, and stained with BM Purple AP substrate or 1 × NBT/BCIP (Roche Applied Sciences) at RT in the dark, overnight if necessary. Stained embryos were washed several times in PBS, fixed in formalin and stored at 4 °C. Some were dehydrated through graded ethanols and Histoclear (National Diagnostics), wax-embedded, sectioned at 7–10 μm and mounted in Immumount (Thermo Scientific).

β-Galactosidase staining

Embryos for wholemount staining (for *Mef2c[AHF]-Cre*, *R26R*^{lacZ} lineage tracing, or *Acvr1*^{nlsLacZ} detection (see below)) were fixed for 15 min in 0.5% glutaraldehyde in DPBS, washed at least three times

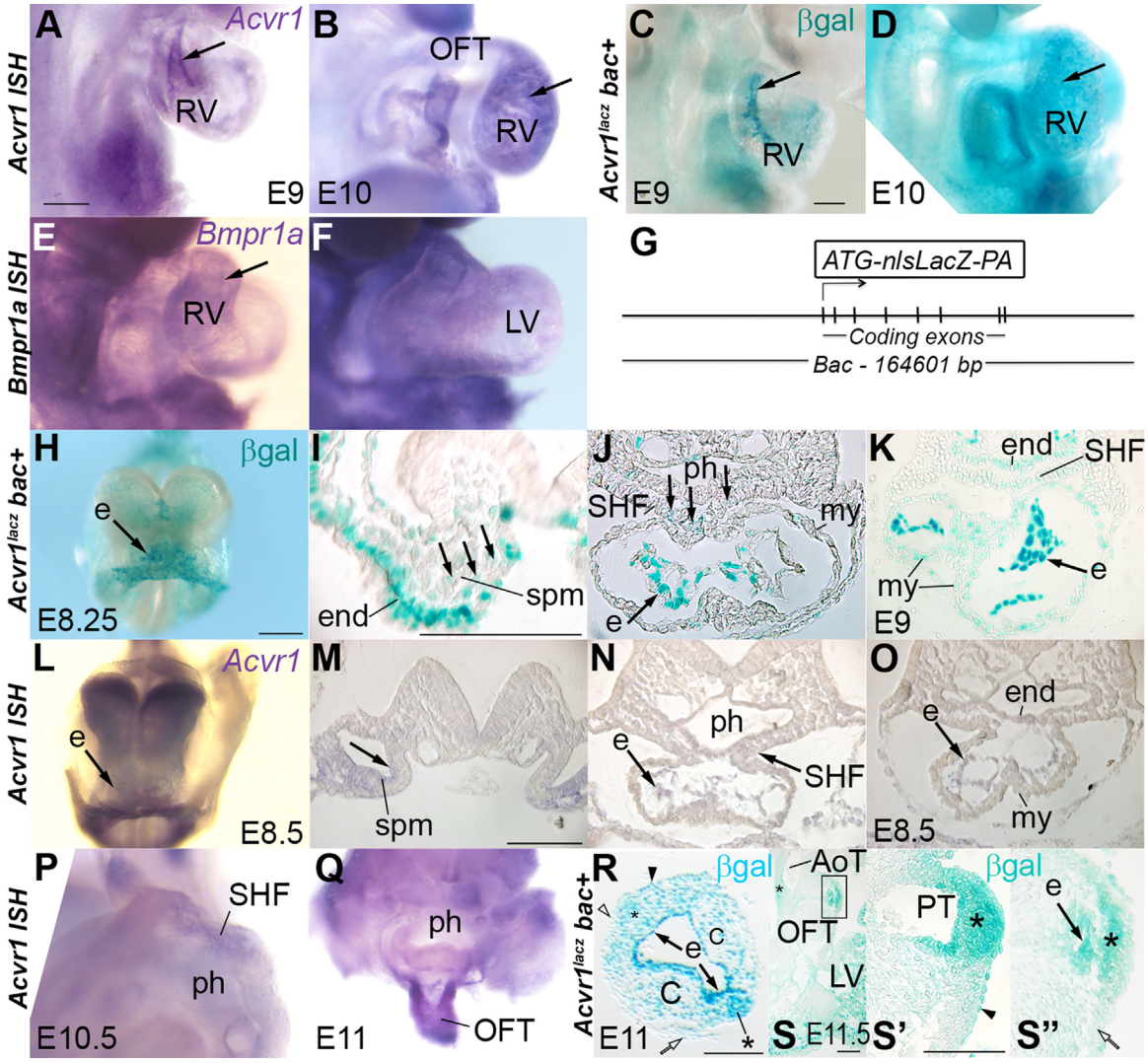

Fig. 5. ***Acvr1*** **is expressed in SHF and endocardium.** A–F, E9, E10 from right except F, apical: Strongest expression of *Acvr1* in endocardium (arrows) but *Bmpr1a* similar level in all cardiac tissues. G, Transgenic bac reporter line construct, *nls-lacz-polyA* inserted in *Acvr1* exon 3. H–O *Acvr1* expression in early anterior (I) and later posterior (M) splanchnic mesoderm (spm, arrows, I,M). Strongest expression in endocardium (e) throughout heart tube from E8.25 (H,J,K,L,N,O). Weaker, intermittant expression in SHF (J, K, N), myocardium (my) and pharyngeal endoderm (end) by E9 (K). J: section from H, M–O: sections from L. P–S″ *Acvr1* expression in mid SHF (P, cut above atrium, viewed from posterior) and distal OFT (rest of heart removed, Q), including morphologically distinct columns of SHF-derived cells (∗), some that contribute to aortic (AoT) and pulmonary trunk (PT) (S–S″). Strong expression in endocardium (e); in neural crest cushion cells (C), some epicardial cells (arrowheads R, S′), less expression in myocardial wall (open arrows). R,transverse, S oblique, sections of distal OFT of WMT βgal-stained E11-11.5. S″ is detail from S, S′ from more distal section. C, cushion; e, endothelium; end, endoderm; my, myocardium; ph, pharynx; spm, splanchnic mesoderm. Scale bar 200 μm, except R′,S, 100 μm.

in detergent rinse, then stained using standard procedures (Hogan et al., 1994). After sufficient staining had occurred, embryos were washed in detergent rinse and PBS and fixed in formalin. Some were processed to wax using Histoclear (National Diagnostics), sectioned at 7 or 10 μm, and mounted in Immumount (Thermo Scientific).

Microscopy and photography

Results were viewed and recorded on an Olympus BX51 (sections, bright field and fluorescence) with Olympus DP71 and software, Leica MZ95 microscope (wholemount or sections, bright field) with Olympus DP72 and software, or Leica M165FC (wholemount, brightfield) with DP73 and software. A dish of agarose was used to obtain consistent orientations of small tissues. Adobe Photoshop 4 and 6 were used to invert immunofluorescence images and prepare figures for publication according to editors' requirements.

Sample recovery for quantitative RT-PCR

Second heart field cells were recovered by FACS from *Mef2c-Cre*$^{+}$, *R26R*$^{YFP/WT}$ E9 and E10 torsos (from which the heart tube had been completely removed), cut between first and second pharyngeal arches distally and immediately anterior to the atrial position posteriorly. Each torso piece was digested in 1% Collagenase I (Worthington) diluted 1:9 with Hanks BSS for 15–20 min at 37 °C, pipetted gently to disperse cells, cell-strained and stored on ice before sorting using the GFP channel on a Beckman Coulter MoFlo Astria Cell Sorter. Cells from each sample were collected directly into 500 μl of RLT (Qiagen) to which 20 μl of 1M DTT was added, transferred to 1.5 ml tubes and stored at −80 °C. RNA was purified using RNeasy (Qiagen) and Omniscript (Qiagen) used to make cDNA. RT-PCR was used to confirm the genotype of each sample (data not shown).

'RV+OFT' tissue was dissected from E9 embryonic hearts by cutting across the OFT immediately adjacent to the second heart field distally and through the interventricular groove/inner curvature

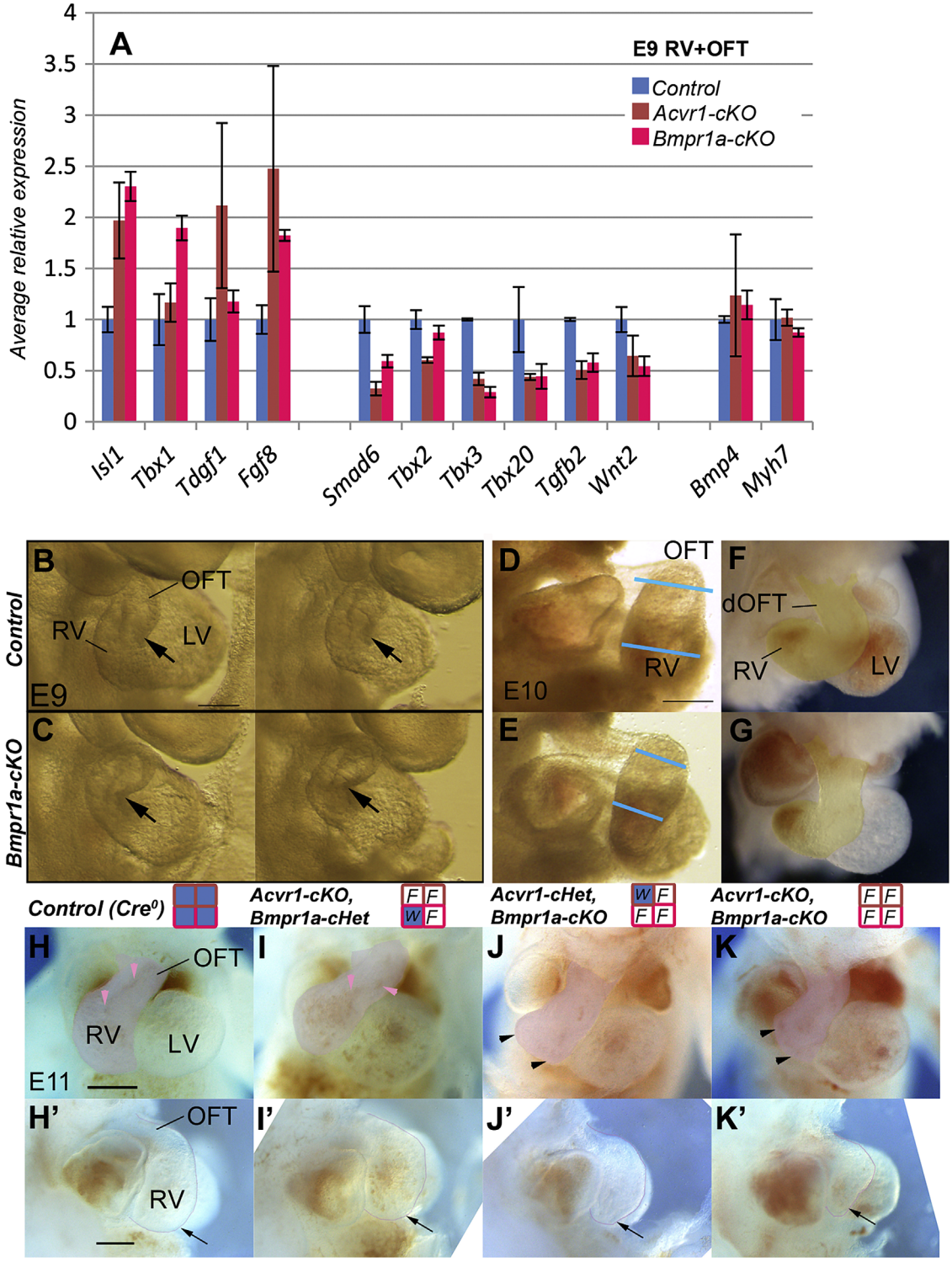

Fig. 6. Effect of *Bmpr1a-cKO* on gene expression in OFT/RV and on OFT/RV development. A, qRT-PCR on E9 RV+OFT: *Bmpr1a-cKO* RVOFT tissues (pink bars) showed similar differences in selected gene expression to those of *Acvr1-cKO* (red bars) relative to controls (blue). However, *Tbx1* was more highly expressed in *Bmpr1a-cKO* mutants. *Tdgf1* and *Tbx2* in *Bmpr1a-cKOs* differed very little from controls. *$p \leq 0.05$ *Bmpr1a* control vs cKO. B–G, E9, E10 hearts, B–E from right, F–G 4-chamber. At E9, RV (arrow) in two representative *Bmpr1a-cKO* hearts (B) appeared narrower vs OFT than those of controls (C)(RV+OFT of these samples used for qRT-PCR). At E10, RV appeared wider in control (D,F) than mutant (E,G) though OFT of similar width (blue lines in D,E; RV and OFT colored yellow in F,G). H–K′, Progressive loss of BMP Type I receptor alleles increased abnormality in size and shape of RV, and OFT at E11. Functional (blue) alleles remaining following *Mef2c[AHF]-Cre* recombination indicated in grid by title: top row, *Acvr1*; lower row *Bmpr1a*; *W*, *wild type*; *F*, *floxed*. Arrow (H′–K′) marks position of anterior face of posterior RV which appeared progressively narrower, and flattened apically (arrowheads, J,K). One *Bmpr1a* allele appeared more effective at maintaining RV than one *Acvr1* allele. OFT also became shorter (J′,K′) and narrower (K). Straight RV outlet route visible (pink arrowheads) in control (H) but twisting in mutant (I). H, K 4 chamber view, RV+OFT colored pink; H′–K′ view from right, RV+OFT outlined. dOFT, distal OFT. Scale bar 200 μm.

proximally. Each sample was immediately placed in a separate labeled 1.5 ml tube, excess DPBS removed, and 100 μl RLT buffer (Qiagen) added. Samples were stored at −80 °C until RNA isolation. RNA was isolated using RNeasy micro kit (Qiagen) following

manufacturer's instructions. All 12 μl of RNA solution was immediately used to make 20 μl cDNA using Omniscript (Qiagen) and random primers (Life Technology), and stored at −20 °C. To increase the number of different gene expressions that could be assessed on the *Acvr1,Mef2c-Cre* samples, pre-amplification was performed using the TaqMan Pre Amp master mix (Applied Biosystems) according to manufacturer's instructions: sense and antisense primers used in the Roche Universal system (see below) for qRT-PCR were diluted to the correct concentration and used in place of TaqMan assay reagents. Ten cycles of pre-amplification were performed on 1 μl of cDNA per 20 μl reaction, and the resulting solutions diluted 1:5 with TE, and stored at −20 °C. Assays on cDNA and pre-amplified DNA were used to confirm that relative quantification was unaltered following pre-amplification (data not shown).

Real time quantitative PCR

Most experiments were carried out using Universal Probe Library-based assays (Roche Applied Science) with gene-specific primer sequences generated by the manufacturer's online algorithm and TaqMan Universal PCR master mix (Applied Biosystems) (see Supplemental Table 3 for sequences). Some used Taqman Assay reagents (see Supplemental Table 3). 30 μl assays were quantified using Applied Biosystems ABI7300 PCR and ViiA7 detection systems and software. All Ct values were checked by eye. *Actb* levels were used to normalize other expression levels. cDNA was diluted to avoid Cts lower than 18. At least three separate control (Cre negative or conditional heterozygote) and three separate mutant samples were assessed for each genotype/condition, where possible from the same litter, or at least stage-matched.

miRNA assays

Individual E9 RV+OFT pieces were dissected manually as described above and stored in QIAzol lysis reagent (Qiagen) at −80 °C until RNA isolation using miRNeasy mini kit (Qiagen). Individual E9 second heart field-enriched torso pieces without heart were dissected manually and stored at −80 °C until RNA isolation using miRNA purification kit from Norgen Biotek. After quantification, samples were shipped overnight on dry ice to LC Sciences (Houston Texas) who assayed the samples miR-17 and miR-20a (using Taqman miRNA assays Ids 2308, 0580) and control RNAs snoRNA202 and noRNA234 (assay Ids 1232, 1234). Three stage-matched pairs of controls and mutants were used for each genotype assayed; each of these assayed in triplicate for each assay, along with a no template control.

Statistical analyses

For histological and expression (qRT-PCR) analyses three or more samples were analyzed unless otherwise stated. Averages, standard error and probability (Student's t-test, 1-tailed) were calculated. Probability (*P*) equal or less than 0.05 was marked as significant.

Results

Acvr1 in the AHF is required for OFT septation and RV development

To address the role of the BMP type I receptor AcvRI in the SHF, *Acvr1* was deleted using *Mef2c[AHF]-Cre*$^{+}$ driver mice (Verzi et al., 2005). The resulting *Acvr1*$^{F/F}$*/Mef2c[AHF]-Cre*$^{+}$ embryos (*Acvr1-cKO*) lacked most of the functional *Acvr1* in the *Mef2c[AHF]-Cre* recombination domain (Online Fig. 1).

Defects in post-septation stage Acvr1 mutants

Acvr1-cKO embryos consistently had morphological defects in ventricular and OFT septation (Fig. 1A–Fb). Membranous ventricular septal defects (VSD; Fig. 1Fa, Fb) were accompanied by OFT, valve and aortico-pulmonary (AP) trunk septation defects that formed a spectrum in severity, from the mildest, DORV (double outlet right ventricle, Fig. 1Da, Ea, Fa) to CAT (common arterial trunk, from which pulmonary arteries arose directly posteriorly). In some examples of CAT, septation of the arterial valves had not occurred, but two trunks of similar size (Online Fig. 2), or one rudimentary (Fig. 1Eb, Online Fig. 2Lb), were present distally. Despite these malformations, six (or more) OFT valve cushions/leaflets could often be identified in partially or distally unseptated CAT, and coronary ostia were grossly normal (Online Fig. 2). Defects in arterial tree downstream, and atrial/AV septation upstream were sometimes found but were not further examined in this study.

Defects in pre-septation stage Acvr1 mutants

Acvr1-cKO hearts could usually be distinguished morphologically from controls between E9 and E11 especially by a smaller RV apex (Fig. 1G–N): The inner curvature could also appear narrower (Online Fig. 3A, B). A reduction in Bmp signaling could be detected in recombined *Acvr1-cKO* heart cells at E9 (Fig. 1I,J) and the myocardium of these phenotypically abnormal structures was all recombined by *Mef2c[AHF]-Cre* (Fig. 1L,O). Unrecombined regions in control and *Acvr1-cKO* hearts appeared morphologically indistinguishable (Fig. 1 and data not shown).

It has been suggested that the appropriate degree of OFT 'rotation' is required to position aortic and pulmonary trunks with respect to the ventricular outlets and ventricular septum appropriately (Bajolle et al., 2006), which can be defective when BMP signaling is compromised (Beppu et al., 2009). At E12, mutant OFTs were found to be (variably) less 'rotated' as judged by the angle of the opposing faces of the parietal and septal cushions to the embryonic anterior–posterior (A–P) axis (Fig. 1Q–Tb). *Sema3c* expression, strongest in sub-pulmonary myocardium which should be anterior by E12 (Theveniau-Ruissy et al., 2008), was also abnormal at E11 and 12 in mutants (Fig. 1U–Z).

Other regional differences in wall morphology were also present in mutants. By E10, mutant OFT wall was more varied in thickness (Online Fig. 3C–H): the anterior face of the mid-proximal OFT wall appeared thicker, and an area of much thinner wall on the posterior/left side of mutant OFTs surrounded part of the septal cushion (Online Fig. 3I–W). The wall cells in the thin region appeared to contain much less cytoplasm and less, poorly organized, striated muscle myosin than those in other parts of the wall, or control cells, (Online Fig. 3O,P). Despite this, the cells were typical of wall, not mesenchymal cell phenotype, as they were Isl1- and SMαA-positive, and Sox9-negative (Online Fig. 3I–L). Some apoptosis was present nearby but not localized within the thin wall itself (Online Fig. 3R–S). This area was barely overlain by epicardium by E12 (Fig. 3T,U). The right ventricular wall did not appear to differ in thickness between mutants and controls, and its trabeculation was not grossly abnormal (data not shown).

Mesenchymal cells are added to the initially cell-free ECM cushions along the length of the OFT both distally (by migration of CNCC via the pharyngeal region) and locally, especially proximally, through EMT from overlying endocardium. At E11, instead of the usual 2(+2) cushion arrangement, *Acvr1-cKO* mutants had highly populated cushions of differing sizes mid-OFT, and a single mesenchymal cushion usually packed to one side distally (Fig. 2A–C,F–H) in which mesenchyme underwent more cell death at E12 (Online Fig. 4Q–T). The lumen(s) formed by these cushions were tortuous, and the endocardium itself was irregular in contour (Fig. 2F–I).

Proximally, mutant cushions were abnormally shaped, and cushion continuity to AV cushion absent (Fig. 2D,E,I,J). Cushion mesenchyme organization was abnormal and *Plexina2* expression (expressed by CNCC) reduced in mutants (Fig. 2K–S). Recombined endocardium appeared to make little contribution to cushion mesenchyme (Fig. 2N,T), so CNCC likely contributed most of the mesenchyme as endocardium appeared increasingly recombined during this period. Consistent with this, Smad1/5/8 phosphorylation was clearly detectable in both control and mutant OFT mesenchyme at E11 (Fig. 2O,U). OFT cushion morphology was frequently so abnormal in *Acvr1-cKO*

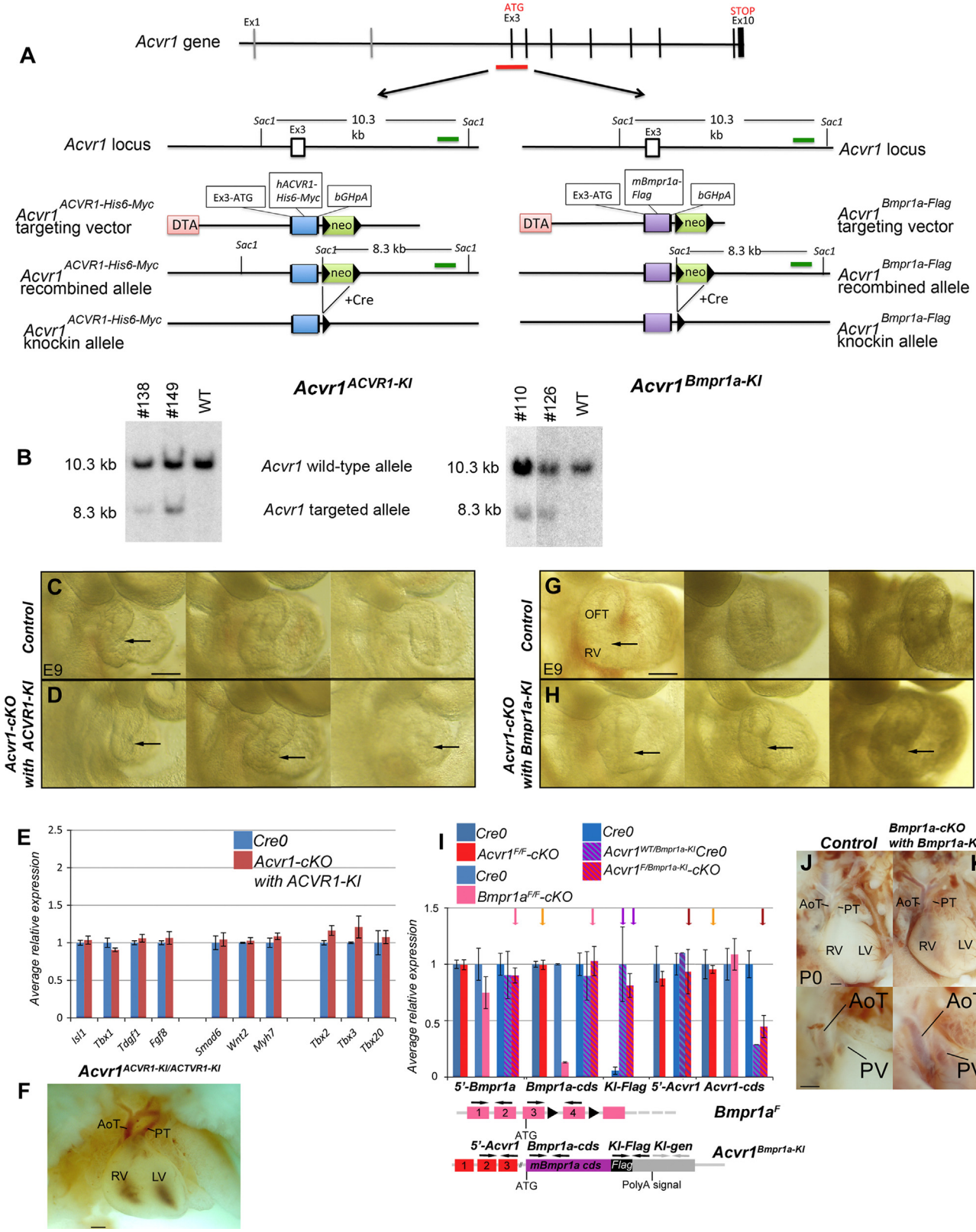

that two separate lumens were not maintained through them to the aortic sac (Fig. 2G, Online Fig. 4F), so they would not have aligned with the nascent aortic and pulmonary trunk flow routes distally if formed. Distal SHF-derived OFT and aortic sac wall morphology was abnormal. A recognizable column of Isl1-positive, MF20-negative SHF cells on the posterior/left of the distal OFT showed variably reduced phospho-Smad1/5/8 immuno staining (Fig. 2O,U) and abnormal morphology in mutants, and lay adjacent to the area of thin myocardium (Online Fig. 4A–L).

These results show that AcvR1 in SHF-derived cells made an essential contribution to the development of structures important for ventricular, OFT and AP septation, and that its removal affected the behavior of both SHF-derived cells themselves (myocardium and endocardium) and those genetically normal with which they interact (CNCC).

Loss of Acvr1 in the SHF results in altered gene expression, increased cell proliferation and altered regional identity in OFT myocardium

To investigate molecular pathways underlying the effects of removing AcvR1 function, we chose to study E9, as later events may be secondary to earlier regulatory defects, and the more complex anatomy make it harder to discriminate different processes.

Chick anterior SHF explant studies suggest that FGFs and BMPs co-ordinate the balance between proliferation and differentiation of anterior SHF progenitors, in part by inhibiting one another via distinctive groups of 'synexpressed' genes (Hutson et al., 2010; Tirosh-Finkel et al., 2010). Cardiomyocyte and smooth muscle precursors continue to be added to the mouse heart tube from the anterior SHF between days 9 and 12 (reviewed by Vincent and Buckingham (2010)) so to determine if AcvRI-mediated BMP signaling mediates FGF repression in anterior SHF progenitor cells themselves, we assessed their gene expression by qRT-PCR at E9 and E10 in FACS-sorted populations purified from individual *Mef2c[AHF]-Cre*-positive *Acvr1*$^{F/WT}$ (control) and *Acvr1*$^{F/F}$ (cKO, mutant) embryos heterozygous for *R26R-YFP*. The results (Fig. 3A) were consistent with BMP signaling being reduced in mutants but FGF synexpression only slightly affected. We also assessed other genes implicated in SHF-derived heart tube development, *Isl1*, *Tbx1*, *and Fgf10* (Cai et al., 2003; Watanabe et al., 2012; Xu et al., 2004) (Fig. 3A). Average *Tbx1* expression was higher at E9 and *Isl1* expression less by E10, in mutants.

AcvR1 might still have mediated *Fgf* repression in anterior SHF-derived cells that have joined the heart tube itself, so we compared the expression of these and other genes implicated in regulating proliferation and differentiation in the RV/OFT segment of individual control and mutant heart tubes at E9 (Figs. 3B–G and 4A–G). BMP signaling was reduced in recombined mutant RV/OFT relative to controls (Fig. 1I,J). Only *Fgf8* expression was much higher in mutants, (not *Fgf10*, or other synexpression genes, Fig. 3B, E–F), but the abnormal expression of a number of other markers in mutants was consistent with a continued proliferative/less-differentiated phenotype: *Isl1*, *Tdgf1*, *Tbx1*, *Wnt2* (Figs. 3B,G; 4A–D). A delay in differentiation did not extend to average sarcomeric muscle gene expression which was little altered for those encoding functionally important quantities (Fig. 4A). Although *Nppa* levels were on average lower in mutants (data not shown), WMT ISH showed not only that *Nppa* expression was still present in RV trabeculations, but ectopic patches were present distally beyond the RV chamber and more widely around the circumference of the OFT at E9, 10 and 11 (Fig. 4F, Online Fig. 4A–C, data not shown). *Nppa* expression is normally restricted to the 'chamber' myocardium of the ventricles and atrial appendages and does not occur in AV junction or OFT myocardium. The boundary between phenotypic chamber and non-chamber in AV region heart myocardium is tightly regulated by Tbx2, Tbx3, and Tbx20 (Cai et al., 2005). These may play a similar role in OFT (Mesbah et al., 2012; Ribeiro et al., 2007; Sakabe et al., 2012). Expression of these (BMP-target) genes was reduced in mutants, as was another regional marker, *Tgfb2* (Fig. 4E,G). Proliferation is normally low in non-chamber AV region myocardium, but was higher on average in mutant vs control OFT (Fig. 4H). Note that average expression of *Bmp4* and *Bmp2* at E9 was not reduced (Fig. 4E), so their signaling through other receptors, and in non-recombined cells (such as neural crest cells) would not be expected to be reduced.

Stabilization of β-catenin did not substantially rescue Acvr1-cKO phenotype

Embryos lacking *Ctnnb1* in SHF have very small RV, CAT and dysmorphic OFT cushions (Ai et al., 2007). We therefore wondered whether any relevant Wnt/Ctnnb1 signaling lay downstream of Bmp signaling and tested this by stabilizing canonical Wnt signaling by maternal LiCl injection (Tian et al., 2010). A number of genes showed some normalization in average levels in treated embryos, suggesting β-catenin signaling might normally act downstream of AcvR1-mediated BMP signaling to regulate *Fgf8*, *Tgfb2*, *and Ccnd2* expression. *Tbx3*, *Tbx20*, *Isl1*, and *Wnt2* expression remained abnormal, and LiCl-treated *Acvr1-cKO* hearts also remained macroscopically morphologically abnormal at post-septation stages (Online Fig. 5).

Fig. 7. Generation and analysis of mice carrying the *Acvr1*$^{ACVR1-}$ and *Acvr*$^{Bmpr1a-}$ knock-in alleles. Note that, for ease of reading, these knock-in alleles are sometimes referred to as *ACVR1-KI* (rather than *Acvr1*$^{ACVR1-KI}$) and *Bmpr1a-KI* (rather than *Acvr1*$^{Bmpr1a-KI}$) in Figs 7 and 8. A–B, Construction of *Acvr1*$^{ACVR1-}$ and *Acvr1*$^{Bmpr1a-}$ knock-in alleles. A: A segment of the first coding exon (3) and next donor splice site of *Acvr1* was replaced by Myc-tagged *ACVR1* cDNA (left panel) or Flag-tagged *Bmpr1a* cDNA (right panel). B: Targeted ES-cell clones were first identified by PCR (data not shown) and the correct targeting was confirmed by Southern blotting. DNAs isolated from control (WT) ES cells and putative correctly targeted ES cell clones (#138 and #149 for *Acvr1*$^{ACVR1-KI}$, left panel; #110 and #126 for *Acvr1*$^{Bmpr1a-KI}$, right panel) were digested with *Sac*I and detected with an external probe (green bar in A). The wild-type and targeted alleles show 10.3-kb and 8.3-kb *Sac*I fragments, respectively. C–D, E9 hearts from right: Comparison of RV, OFT morphology of three representative control (C: *no Cre*) and *Acvr1*-cKO with *ACVR1*-KI mutant (D: *Acvr1*$^{F/ACVR1-KI}$, *Mef2c[AHF]-Cre*$^{+}$) embryos, showing similar range in size of right ventricle in mutants as controls (arrows). RV + OFT of these samples used for qRT-PCR shown in E. E, qRT-PCR on E9 RV + OFT *Cre*^{0}, *Acvr1*$^{ACVR1-KI}$-negative controls (blue), *Acvr1* $^{F/ACVR1-KI}$-cKO mutants (red columns). In contrast to *Acvr1*$^{F/F}$-cKO (Fig. 3) and *Acvr1*$^{F/Bmpr1-KI}$-cKO (Fig. 8A), average gene expression in mutants is the same or very similar to that in controls. Each bar average of 3 separate samples, ± SEM. F, E15 4-chamber view of heart in *Acvr1*$^{ACVR1-KI/ACVR1-KI}$ embryo showing normal gross morphology, including complete AP septation. G–H, E9 hearts from right: Comparison of RV, OFT morphology of three representative control (G: *no Cre*) and *Acvr1*-cKO with *Bmpr1a*-KI mutant (H: *Acvr1*$^{F/Bmpr1-KI}$ *Mef2c[AHF]-Cre*$^{+}$) embryos, showing variable reduction in size of right ventricle in mutants (arrows). RV + OFT of these samples used for qRT-PCR, Fig. 6 A,B. I, qRT-PCR on E9 RV + OFT of various controls and mutant genotype samples. We assessed relative levels of *Acvr1*$^{Bmpr1a-KI}$ expression in three ways. Transcripts from *Acvr1*$^{Bmpr1a-KI}$ were specifically detectable (using '*KI-Flag*' primers) in *Acvr1*$^{Bmpr1a-KI}$ control and mutant samples (purple arrows). The presence of one *Acvr1*$^{Bmpr1a-KI}$ allele in mutants increased the average level of *Bmpr1a* by only 14% (compare the results (pink arrows) of '*Bmpr1a-cds*', which detects both *Bmpr1a* and *Acvr1*$^{Bmpr1a-KI}$, and '*5′-Bmpr1a*', which only detects *Bmpr1a*). This suggests that only a subset of cells would have experienced supra-normal levels of Bmpr1a. Loss of signaling via Acvr1 did not alter the average amount of either *Acvr1* or *Bmpr1a* RNA (orange arrows). *Acvr1*$^{Bmpr1a-KI}$ >allele was expressed at about the same level as *Acvr1*^{WT} **or *Acvr1*^{FI}**: It includes 5′UTR exons from *Acvr1* but not the *Acvr1* cds. The relative level of *Acvr*1 5′UTR remained the same in samples with or without an *Acvr1*$^{Bmpr1a-KI}$ allele, whereas the level of '*Acvr1* cds' detected was halved when one of the *Acvr1* alleles was *Acvr1*$^{Bmpr1a-KI}$ (brown arrows). These results also suggest that the levels of expression driven by the *Bmpr1a* locus and *Acvr1* locus may differ (and vary with cell type: see Fig. 5). Genomic DNA contamination (assessed using '*KI-gen*' primers) did not contribute (data not shown). J–K P0 4-chamber, and oblique right view below: Gross morphology and trunk (AoT, PT) septation in *Bmpr1a-cKO* also carrying one *Acvr1*$^{Bmpr1a-KI}$ allele (K) very similar to Cre^{0} control (J). AoT, aortic trunk; cds, coding sequence; OFT, outflow tract; PV, pulmonary valve; RV, right ventricle. Scale bar 200 μm (C,D,G,H) or 500 μm (F,J,K).

Do AcvR1 and BmpR1a regulate the same pathways and processes in anterior SHF-derived cells?

Both AcvR1 and BmpR1 are BMP Type I receptors, yet abnormal development occurs if the expression of one of these genes is deleted from the anterior SHF. This may be because they are expressed in different physical or chronological domains, and/or that each controls distinctive regulatory events. Using RNA WMT ISH and a novel *lacZ-bac* line to report *Acvr1* expression, we found expression in SHF and heart tube cells, as reported for *Bmpr1a* (Klaus et al., 2007; Song et al., 2007) but whilst *Bmpr1a* was broadly expressed at similar levels (Fig. 5E,F), *Acvr1* was most strongly expressed in endocardium, and cushion mesenchyme (Fig. 5A–D, H, K–O, R). Weaker expression was also found in splanchnic lateral plate mesenchyme, variably in SHF

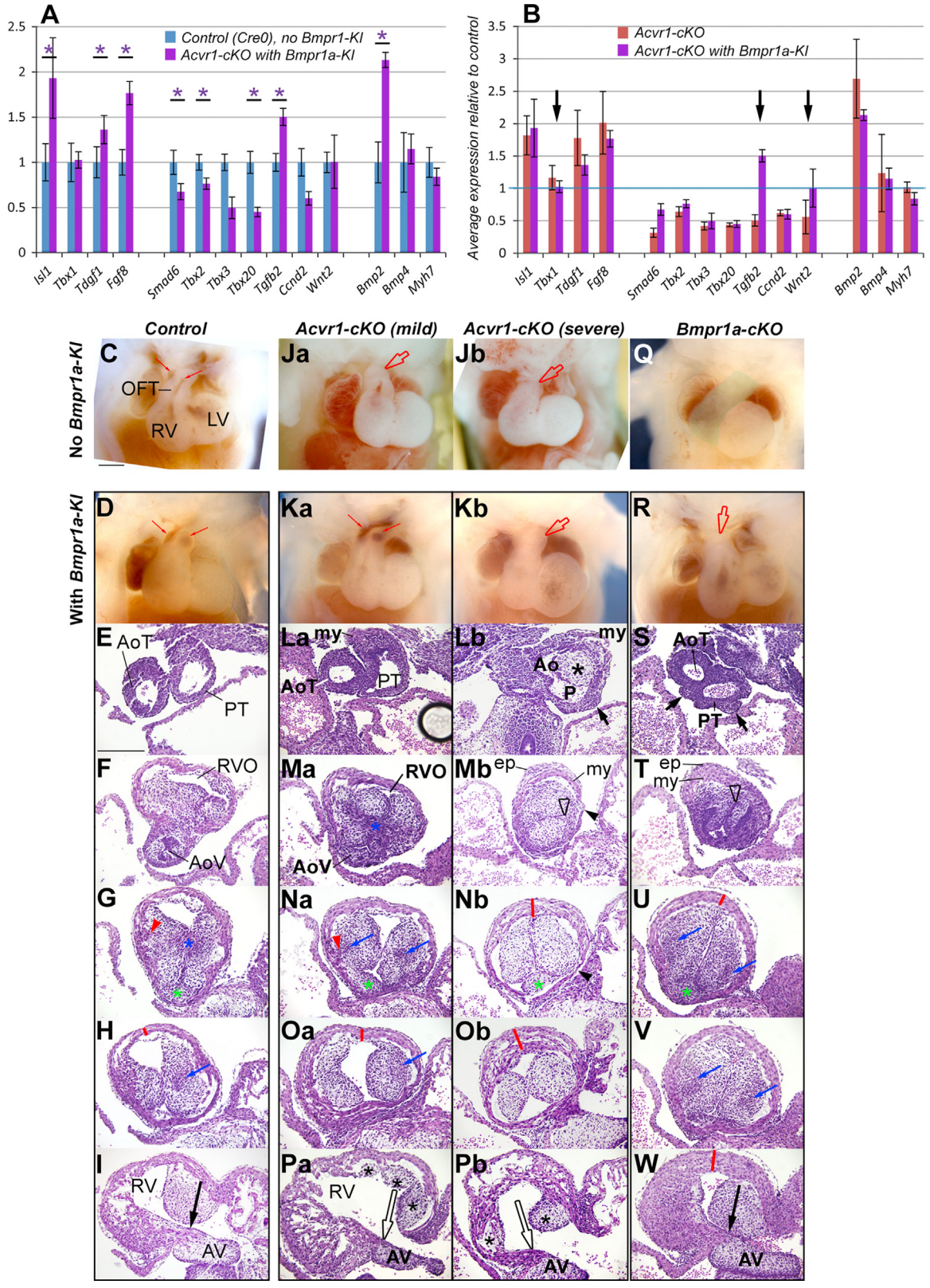

cells and gradually increasing in myocardial cells after tube formation. It was detectable in SHF cells at E10 and in non-myocardial OFT cells at E11 (Fig. 5H–S′).

We also found that most of the genes showing altered expression in *Acvr1-cKO* RV+OFT at E9 were similarly altered in *Bmpr1-cKO* (Fig. 6A). The morphological phenotype of *Bmpr1-cKO* was also similar, but more extreme (compare Fig. 1H vs 6C, and Online Figs. 3 and 4 vs 6) including small RV (E9-10), abnormal OFT cushion development, abnormal OFT wall and CAT-consistent morphology at E12. All were dead by E13. Hearts containing only one or no *Acvr1/Bmpr1a* alleles also showed progressively more abnormal RV and OFT phenotypes (Fig. 6H–K′), so mal-development might be the result of a lack of sufficient BMP Type I receptor capacity remaining for normal development if only either *Acvr1* or *Bmpr1a* were absent. To test this, we added *Bmpr1a* and *ACVR1* back in place of *Acvr1* genetically in *Acvr1-cKO* mice by making two novel knock-in mouse lines carrying an *Acvr1* allele in which either *Bmpr1a* cDNA (to make $Acvr1^{Bmpr1a\text{-}KI}$) or *ACVR1* cDNA (to make $Acvr1^{ACVR1\text{-}KI}$) coding sequence under *Acvr1* locus control replaced the endogenous *Acvr1* sequence (Figs. 7 and 8). $Acvr1^{ACVR1\text{-}KI}$ allele ('*ACVR1A-KI*') functioned similarly to $Acvr1^{WT}$, and the presence of $Acvr1^{Bmpr1a\text{-}KI}$ ('*Bmpr1a-KI*') was not lethal, as $Acvr1^{ACVR1\text{-}KI/ACVR1\text{-}KI}$ homozygote knock-in, $Acvr1^{Bmpr1a\text{-}KI/ACVR1\text{-}KI}$, $Acvr1^{WT/Bmpr1a\text{-}KI}$ and *Cre*-negative $Acvr1^{F/Bmpr1a\text{-}KI}$ animals were viable, fertile and grossly normal (data not shown), and $Acvr1^{ACVR1\text{-}KI/F}$*-cKO* resembled Cre-negative controls in morphology and E9 RV+OFT gene expression (Fig. 7C–F). However, only limited normalization of average gene expression was found in E9 *RV+OFT* from $Acvr1^{Bmpr1a\text{-}KI/F}$*-cKO at E9: Tbx1* and *Wnt2* to control levels, *Smad6* partially restored, and *Tgfb2* from under-expression to over-expression (Fig. 8A,B). From E12, these embryos still displayed a spectrum of septation defect phenotypes ranging from CAT to successful AP septation (Fig. 8, Table 1), but with variable normalization of mid-OFT cushion orientation, organization and number, and restoration of OFT wall thickness (Fig. 8La–Pb). This was despite the fact that expression of $Acvr1^{Bmpr1a\text{-}KI}$ RNA could be detected at E9 (Fig. 7I), and produced functional protein as there was some improvement in average *Smad6* expression at E9, and *Bmpr1a*-cKO, $Acvr1^{WT/Bmpr1a\text{-}KI}$ mice survived beyond E13 and showed a substantial improvement in morphology (Fig. 7J,K, Fig. 8Q–W, Table 1).

We therefore conclude that AcvR1 and BmpR1 each mediate signaling required for normal development in the anterior SHF-derived tissues, and propose that the abnormalities that arise from the deletion of either gene may result in part from a Tbx2/3/20-mediated mis-regulation of the regional identity of the OFT myocardium. Despite the similarities in their location and in the effects of their absence, AcvR1 and BmpR1a play some non-redundant roles in the development of anterior SHF-derived cardiovascular tissues.

Discussion

Implications for BMP-dependent arterial pole cardiovascular morphogenesis

In this, the first report of the *Acvr1* arterial pole *cKO* phenotype, we have shown that a spectrum of SHF-related cardiovascular septation defects occurred but survival was possible to birth. Analysis of morphology at different times and positions along the OFT suggests a model in which the degree of distal (aorticopulmonary trunk) septation is in part dependent on the correct positioning of two nascent OFT lumens in relation to those formed by the most distal component of the septation complex, a neural crest-dependent protrusion in the dorsal wall of the aortic sac, which lies between the routes to pharyngeal arch III,IV vessels and arch VI vessels. Loss or mis-positioning of one lumen means that a permanently unseptated truncal region, even if more distal septation still occurs. The mechanism underlying the variability is still unclear but key morphological features of normal and abnormal development of this region, and similarity to human congenital malformations of the variety of abnormal phenotypes we saw in *Acvr1-cKO* are examined in detail in Anderson et al. (2012).

We detected reduced Bmp signaling via Smad1/5/8 phosphorylation in recombined OFT wall cells at both E9 and E11, but it is not possible solely from this approach to determine which events are key to normal morphogenesis without considering morphological evidence. Pre-septation, we found that OFT 'rotation' was less than normal, and that OFT wall morphology was regionally abnormal. This could be because specific SHF populations failed to make their normal contribution to the OFT. RV/OFT walls are formed from cells originating in different areas of SHF (Bertrand et al., 2011; Dominguez et al., 2012; Takahashi et al., 2012) and their regional contribution to the tube may act to displace others in relation to the axes of the rest of the heart, i.e., relative 'rotation' (Bajolle et al., 2006; Scherptong et al., 2012), including forming the distinctive subpulmonary myocardial population essential for normal truncal origin position and proximal trunk wall cells. We observed consistent regions of abnormally thin and thick OFT walls, areas of thickened trunk wall, and an insufficiency of sub-pulmonary myocardium suggesting AcvR1 and BmpR1a-mediated BMP signaling is required for normal formation, location and differentiation of specific SHF cell populations. Both OFT wall thickness and 'rotation' were improved by adding *Bmpr1a-KI* expression to *Acvr1-cKOs* consistent with the rescue of a related 'thin wall' model (Wang et al., 2010).

OFT cushion morphology is important for OFT septation but also affected lumen position and number in both *Acvr1-* and

Fig. 8. Effect of *Bmpr1a* knock-in into *Acvr1* locus (*Bmpr1a-KI*) on gene expression and OFT morphology. A, qRT-PCR on E9 RV+OFT: controls (*no Cre*, *no Bmpr1a-KI*), blue columns; *Acvr1-cKO* with *Bmpr1a-KI* mutants (i.e. $Acvr1^{F,\ Bmpr1a\text{-}KI}$, *Mef2c[AHF]-Cre*$^{+}$), purple columns; and B, *Acvr1-cKO* (red columns) vs *Acvr1-cKO* with *Bmpr1a-KI* (purple columns) showing that when Acvr1 was replaced by expression from one allele of *Bmpr1a* cDNA in the *Acvr1* locus average *Tbx1* and *Wnt2* expression became normal, and *Tgfb2* expression was over rather than under expressed (arrows) but expression of other genes shown remained only partially normalized (*Smad6*) or abnormal in a similar way to *Acvr1 cKO*. Each bar average of 3, ± SEM, $^{*}p \leq 0.05$. E12 4-chamber views: Gross morphology of control, mild and severe *Acvr1-cKO* and *Bmpr1a-cKO* without (C, Ja, Jb, Q) and with *Bmpr1a-KI* (D, Ka, Kb, R) dissected to reveal trunks where possible. Presence of *Bmpr1a-KI* in Acvr1-*cKO* improved morphology of RV, OFT in some (Ka vs Ja) but not all (Kb vs Jb) embryos, enlarging RV size and improving OFT orientation (R vs Q, green area) in *Bmpr1a-cKO*. Blood in arterial trunks shows septation in controls and mild *Acvr1-cKO* (Ka). E12 sections, transverse to OFT, H&E: Control (E-I), *Acvr1-cKO* mild (Ka–Pa) and severe (Kb–Pb) phenotype and *Bmpr1a-cKO* (R–W), all with *Bmpr1a-KI*. OFT, from arterial trunk level (top row, sections) to proximal OFT (bottom row). In presence of *Bmpr1a-KI*, all *cKO* showed some improved wall thickness and cushion organization; but uneven wall thickness and distal epicardium (ep) was still seen where distal septation failed. In mild *Acvr1-cKO* with *Bmpr1a-KI*, trunk septation and mid-OFT cushion formation including condensed areas (blue*, arrows), myocardial growth into cushion (red arrowhead) more similar to control, but proximal cushion morphology (black*) and continuity with AV cushion (open arrow, Pa) absent. In the severe mutant with Bmpr1-KI, trunk septation failed (Lb), uneven trunk wall (Lb, short arrow), RVO lumen displaced (open arrowhead), distal (Mb) and proximal cushions abnormal (Pb), mid- to proximal OFT anterior wall too thick (red lines), some wall very thin (arrowheads Mb, Nb) but mid-OFT orientation relatively normal. In *Bmpr1-cko* with *Bmpr1a-KI*, trunk septation only partial, uneven trunk wall (K, short arrows), separate RVO lumen lost (open arrow) but mid- and proximal orientation, condensation (blue arrows), intercalated leaflet (green*) and proximal cushion continuity with AV cushion (W, black arrow), wall thickness except proximally (red lines) similar to control. Compare with *Acvr1-* and *Bmpr1a-cKO* E12 morphology in Figs. 1 and 2 and Online Figs. 2–4. Spaces between cushions and walls are artifacts. Ao, 'aortic' lumen; AV, atrioventricular cushion; ep, epicardium; my, myocardium; P, 'pulmonary' lumen. Scale bar, 200 μm.

Table 1
Incidence of different arterial trunk/OFT phenotypes.

	Acvr1-cKO	*Acvr1-cKO,Bmpr1a-KI*	*Bmpr1a-cKO*	*Bmpr1a-cKO, Bmpr1a-KI*
2 Trunks[a]	E12-E15: 8 (53%) E12-P0: 17 (40%)	E12-E15: 5 (63%)	E12-E14: 0 (0%)	E12-P0: 4 (100%)[c]
1 Trunk	E12-E15: 7 (47%) E12-P0: 25 (60%)	E12-E15: 3 (37%)	E12 (live): 6 (100%) E13-14 (dead[b]): 15 (100%)	E12-P0: 0 (0%)[c]

Mutant genotype samples were categorized according to number of arterial trunks. 'Two trunk' phenotype includes DORV (where AP and OFT valve septation complete) but also CAT with AP septation variably distal to the level of the valve leaflets (no valve septation). 'One trunk' phenotypes showed no AP septation, such that the pulmonary arteries arose from the back of the common arterial trunk.
Range of stages of embryos include in totals is indicated, with percentage (in brackets) of samples of those stages genotyped as cKO showing that number of trunks. These data include dead embryos/newborns in which genotype and anatomy could be determined.

[a] Complete AP and valve septation was present in two *Acvr1-cKO* embryos, one *Acvr1-cKO* with *Bmpr1a-KI* embryo and two *Bmpr1a-cKO* with *Bmpr1a-KI* embryos.

[b] Although variably necrotic, *Bmpr1a-cKO* mutant anatomy could still be determined at E13-14, and limb and eye morphology resembled that of E12 at the latest. The cause of death was not obviously of cardiac origin. An extra-cardiac explanation for lethality has been suggested (Briggs et al., 2013).

[c] The marked improvement in cardiovascular morphology of *Bmpr1a-cKO* in the presence of *Bmpr1a-KI* contrasts with the more limited effects of the allele on *Acvr1-cKO* anatomy overall. A population of *Mef2c[AHF]-Cre*-recombined cells which expresses both *Acvr1* and *Bmpr1a* normally but in which BmpR1A performs an essential role for embryonic survival that AcvRI cannot, is implied by the survival and development well beyond E12 of otherwise *Bmpr1a-cKO* mice.

Bmpr1a-cKOs particularly distally. The regulation of OFT cushion morphogenesis, size and location remains poorly understood at the molecular level. Certain SHF populations, including those identified by Sizarov et al. (Sizarov et al., 2012) and abnormal in morphology and Smad1/5/8 phosphorylation in our models, might play a role in the maintenance of separate nascent truncal lumens close to the OFT wall, perhaps via effects on OFT cushion morphogenesis. As many endocardial/endothelial cells are also recombined by *Mef2c[AHF]-Cre*, their behavior and signaling may also contribute, especially as cushion shape regulation is sensitive to flow (Colvee and Hurle, 1983; Manner et al., 1993) which might be expected to be abnormal from at least E9 as the right ventricle is abnormally small. However, as AP and valve septation were normal in endothelium-specific *Acvr1-cKOs* (Wang et al., 2005) an isolated role in septation failure is unlikely. Abnormalities in OFT mesenchymal behavior including abnormal (circumferential) alignment, and elevated cell death distally, were found in *Acvr1-cKOs* from E11, but also some degree of normal organization and gene expression (*Plxna2*, Sox9). Although Bmp4 expression has been shown to be important in normal OFT cushion development (Jia et al., 2007), other factors may be abnormal in our model, as average expression of *Bmp4* was normal in mutant tissues at E9, and mesenchyme (mostly genotypically normal CNCC) stained strongly for phospho-Smad1/5/8 at E11, and expressed BMP-sensitive Sox9 in both control and mutants. However, we did see abnormalities in regional expression of *Sema3C* (Bajolle et al., 2008) and elevated levels of OFT *Fgf8* expression may have affected cushion shape and cell number proximally (Sugi et al., 2003). Contribution to OFT cushion mesenchymal cells by EMT from recombined cells in *Acvr1-cKO* appeared reduced at E10, consistent with previous results (Wang et al., 2005). Neural crest cells probably made a greater contribution to cushions including valve leaflets where non-CNCC normally contribute, including to OFT valve leaflets, but proximally, continuity between OFT and AV cushions still formed poorly, contributing to the VSD phenotype in *Acvr1* mutants. The walls over which these usually form are totally recombined by *Mef2c[AHF]-Cre*, and were not well rescued by the addition of *Bmpr1a-KI* expression to *Acvr1* mutants, unlike *Bmpr1a-cKO*, consistent with AcvR1 playing a specific role in their formation.

Role of AcvR1-mediated signaling in regulating gene expression in SHF-derived cells

We did not find strong evidence that an autocrine element of the 'BMP/FGF balance' model (Tirosh-Finkel et al., 2010) in recombined cells contributed to the *Acvr1-cKO* phenotype. However, altered expression levels of other genes implicated in precursor/proliferation (elevated) and differentiation (reduced) were found in E9 RV+OFT *Acvr1* mutants: *Fgf8* (promotes SHF proliferation (Ilagan et al., 2006; Park et al., 2006)), *Isl1* (needed for SHF progenitors (Cai et al., 2003)), and *Tdgf1* (*Cripto*, associated with muscle precursor development/proliferation (Guardiola et al., 2012)) elevated; and *Wnt2* (required for myocardial differentiation (Onizuka et al., 2012; Tian et al., 2010)) reduced. *Fgf8*, *Isl1* and *Wnt2* are all *Tbx1* targets (Liao et al., 2008); average expression of *Tbx1* itself was mildly elevated in E9 SHF, (where it maintains proliferation (Zhang et al., 2006)) so may contribute to their altered expression as they enter the heart tube. Elevated expression of *Tbx1* detected in E9 RV+OFT in *Acvr1*- and *Bmpr1a-cKO* mutants is hard to detect in OFT wall by WMT ISH, but cells present distally by the aortic sac at E9 (Chen et al., 2009) would be included in RV+OFT by dissection. Not only was average *Fgf8*, *Isl1*, and *Tdgf1* expression elevated at E9, but their expression also extended along the OFT more proximally and for longer in time in *Acvr1-cKO*, also 'less differentiated' phenotypes. FGF signaling has also been implicated in the differentiation of distal SHF into arterial smooth muscle of the trunk walls (Hutson et al., 2010). Some 'smooth muscle' genes are normally expressed in early embryonic myocardium (such as *Acta2* (Franco et al., 1999)) so were not assayed, but the higher expression of *Myh11* (even though at a very low level), not normally expressed until E14, may reflect a subtle shift in transcriptional milieu to favor smooth muscle-related fate.

T-box transcription factors, *Tbx2*, *3* and *20* are good candidates to be key downstream targets for AcvR1-dependent BMP signaling and the lack of expression of which could be responsible for the phenotypes we report here in *Acvr1-cKO*. That levels of all three are reduced in our mutants could result in a phenotype where partial loss of any one alone would not. They can be directly up-regulated by BMP R-Smad1/5/8 signaling (Singh et al., 2009; Yang et al., 2006). *Tbx2* and *3* have previously been identified as targets in OFT development in *Bmpr1a/Isl1-Cre-cKO* model (Yang et al., 2006) and *Tbx20* as required for suppression of expression of *Isl1* (Cai et al., 2005) and expression of *Tbx3* in the AV (Cai et al., 2011). Their individual and double *KOs* have smaller RV and abnormal OFT (Mesbah et al., 2012). Study of their roles in AV morphological development have shown that they repress the expression of 'chamber' (i.e., ventricular apex and atrial appendage) region genes, including *Nppa*, morphology (trabeculation) and higher proliferation (Ribeiro et al., 2007); and thereby maintain the presence of cushions and formation of cushion mesenchyme,

through expression of genes such as *Has2* and *Tgfb2*. Average *Tgfb2* expression was also reduced in *Acvr1*- and *Bmpr1a-cKO*, and the *Tgfb2-KO* phenotype also resembles that of *Acvr1-cKO*, including a range of OFT/AP septation defects from DORV to CAT with variable degree of distal trunk septation and failure of cushion fusion (Bartram et al., 2001). Mis-expression of *Nppa* and *Tgfb2*, and thicker anterior proximal OFT myocardium *in Acvr1-cKO* suggest that at least the boundary between the right ventricle chamber and non-chamber mid-proximal areas of the OFT wall was less distinct and OFT non-chamber identity compromised. Higher expression of muscle genes in part of the OFT myocardium together with a reduced contribution by the smaller RV might contribute to the similarity of average muscle gene expression in *Acvr1-cKO* and control samples. Like *Isl1* expression, *Tbx2* and *Tbx3* expression only became abnormal in *Acvr1-cKO* after SHF had joined the heart tube, suggesting an AcvR1-mediated process maintained their expression and *Tbx20* from this point. Despite apparently normal levels of *Bmp4* and higher than normal *Bmp2* at E9, remaining Type I BMP receptors were insufficient to normalize levels of these three genes in *Acvr1-cKO*. There is feedback regulation between these T-box factors (Cai et al., 2011; Dupays et al., 2009; Gavrilov et al., 2013), so *Acvr1-cKO* is an interesting model where all three were reduced but none was absent. Again, the failure in *Acvr1*- and *Bmpr1a-cKO* to establish correct chamber and non-chamber-type regions would represent a failure of normal differentiation.

The effects of elevation of Wnt/beta-catenin signaling (by LiCl injection) or BMP signaling (using *Acvr1* locus-regulated *Bmpr1a-KI* or *ACVR1-KI*) on average gene expression in E9 RV+OFT suggest a variety of regulatory pathways controlled the expression of genes altered in *Acvr1-cKO* (Online Fig. 7). Although *Tbx2,3,20* expression was not normalized, the downstream target gene *Tgfb2* became over-expressed by *Bmpr1a-KI* in *Acvr1-cKO*. This may have enabled the degree of context-dependent improvement in morphological development. Comparison of gene expression at E9 with morphological phenotypes suggests additional genes regulated by AcvR1-mediated signaling remain to be identified, and that more region-specific studies are needed to advance understanding of this complex environment.

AcvR1 as one component of BMP signaling in SHF development

AcvR1 and BmpR1a are the principal Type I BMP receptors expressed in the developing RV and OFT wall. Either one alone is insufficient to maintain normal development in arterial pole SHF-derived structures, or expression of known BMP-Smad target genes such as *Smad6*, *Msx2*, *Id1* and *Bambi* at E9 even though *Bmpr1a* and *Acvr1* are expressed at grossly similar times and places. Nevertheless, they appear to regulate many of the same processes (gene expression, morphogenesis). The sequential loss of their functional alleles appeared to create a somewhat gradient-like of loss of normality of morphology (Fig. 6), and of gene expression (though sensitivity/mechanism varied from gene to gene) (Online Fig. 7). Yet even though $Acvr1^{Bmpr1a\text{-}KI}$ was expressed at E9 (Fig. 7I) and substantially rescued *Bmpr1a-cKO* phenotype despite its expression being restricted to the *Acvr1* expression domain, *Bmpr1a-KI* did not restore expression of all assayed genes to normal levels in *Acvr1-cKO* RV+OFT at E9. Surprising amongst these were *Smad6*, *Tbx2*, *3* and *20*. One interpretation is that AcvR1 and BmpR1a have some non-redundant roles, consistent with their known difference in ligand preference (Macias-Silva et al., 1998), but the similarity of gene expression and phenotypes affected suggest that their signaling also needs to be co-ordinated or combined to be effective. It may also be restricted to a very specific region and time. There is evidence in other models for heteromeric receptor formation (Little and Mullins, 2009; Shimmi et al., 2005), but other mechanisms, such as interaction with as yet unidentified regulatory factors, may be responsible.

AcvR1 in congenital heart disease

Although AcvR1 itself is best known for its constitutively active mutant form that results in fibrodysplasia ossificans progressiva (Shore et al., 2006), the *ACVR1 L343P* allele was identified in a screen of atrioventricular septal defect patients and shows greatly reduced signaling capacity and transcriptional activity (Smith et al., 2009). Abnormalities in a number of genes, the normal expression of which we found dependent on AcvR1 have already been identified as causative of CHD (*TBX20* (Kirk et al., 2007) and *TGFB2* (Gao et al., 2012; Lindsay et al., 2012)), or as potential contributory (*TBX2* (Pang et al., 2013),*TBX3* (Chen et al., 2013), *BMP4* (Goracy et al., 2012), *TDGF1* (Roessler et al., 2008; Wang et al., 2011) and *ISL1* (Stevens et al., 2010)). Even a mildly defective allele of *Acvr1* could influence the expression of many genes known to be required for normal heart development and when in combination with other such alleles of these genes account for cases of CHD. The results reported here illustrate the importance of considering the effect of abnormal, though apparently 'redundant', gene products in the understanding of human CHD.

Sources of funding

This study was supported by the NIH RO1 Grant HL074862 (VK).

Acknowledgments

We thank Wanda Filipiak and Margaret van Keuren (University of Michigan Transgenic Animal Model Core) for preparation of transgenic mice, and Martin White and Mike Pihalja (University of Michigan Flow Cytometry Core).

Appendix A. Supplementary material

Supplementary data associated with this article can be found in the online version at http://dx.doi.org/10.1016/j.ydbio.2014.03.008.

References

Ahn, K., Mishina, Y., Hanks, M.C., Behringer, R.R., Crenshaw 3rd, E.B., 2001. BMPR-IA signaling is required for the formation of the apical ectodermal ridge and dorsal–ventral patterning of the limb. Development 128, 4449–4461.

Ai, D., Fu, X., Wang, J., Lu, M.F., Chen, L., Baldini, A., Klein, W.H., Martin, J.F., 2007. Canonical Wnt signaling functions in second heart field to promote right ventricular growth. Proc. Natl. Acad. Sci. USA 104, 9319–9324.

Anderson, R.H., Chaudhry, B., Mohun, T.J., Bamforth, S.D., Hoyland, D., Phillips, H.M., Webb, S., Moorman, A.F., Brown, N.A., Henderson, D.J., 2012. Normal and abnormal development of the intrapericardial arterial trunks in humans and mice. Cardiovasc. Res. 95, 108–115.

Bai, Y., Wang, J., Morikawa, Y., Bonilla-Claudio, M., Klysik, E., Martin, J.F., 2013. Bmp signaling represses Vegfa to promote outflow tract cushion development. Development 140, 3395–3402.

Bajolle, F., Zaffran, S., Kelly, R.G., Hadchouel, J., Bonnet, D., Brown, N.A., Buckingham, M.E., 2006. Rotation of the myocardial wall of the outflow tract is implicated in the normal positioning of the great arteries. Circ. Res. 98, 421–428.

Bajolle, F., Zaffran, S., Meilhac, S.M., Dandonneau, M., Chang, T., Kelly, R.G., Buckingham, M.E., 2008. Myocardium at the base of the aorta and pulmonary trunk is prefigured in the outflow tract of the heart and in subdomains of the second heart field. Dev. Biol. 313, 25–34.

Bartram, U., Molin, D.G., Wisse, L.J., Mohamad, A., Sanford, L.P., Doetschman, T., Speer, C.P., Poelmann, R.E., Gittenberger-de Groot, A.C., 2001. Double-outlet right ventricle and overriding tricuspid valve reflect disturbances of looping, myocardialization, endocardial cushion differentiation, and apoptosis in TGF-beta(2)-knockout mice. Circulation 103, 2745–2752.

Beppu, H., Malhotra, R., Beppu, Y., Lepore, J.J., Parmacek, M.S., Bloch, K.D., 2009. BMP type II receptor regulates positioning of outflow tract and remodeling of atrioventricular cushion during cardiogenesis. Dev. Biol. 331, 167–175.

Bertrand, N., Roux, M., Ryckebusch, L., Niederreither, K., Dolle, P., Moon, A., Capecchi, M., Zaffran, S., 2011. Hox genes define distinct progenitor subdomains within the second heart field. Dev. Biol. 353, 266–274.
Briggs, L.E., Phelps, A.L., Brown, E., Kakarla, J., Anderson, R.H., van den Hoff, M.J., Wessels, A., 2013. Expression of the BMP receptor Alk3 in the second heart field is essential for development of the dorsal mesenchymal protrusion and atrioventricular septation. Circ. Res. 112, 1420–1432.
Bruneau, B.G., 2013. Signaling and transcriptional networks in heart development and regeneration. Cold Spring Harb. Perspect. Biol. 5, a008292.
Cai, C.L., Liang, X., Shi, Y., Chu, P.H., Pfaff, S.L., Chen, J., Evans, S., 2003. Isl1 identifies a cardiac progenitor population that proliferates prior to differentiation and contributes a majority of cells to the heart. Dev. Cell 5, 877–889.
Cai, C.L., Zhou, W., Yang, L., Bu, L., Qyang, Y., Zhang, X., Li, X., Rosenfeld, M.G., Chen, J., Evans, S., 2005. T-box genes coordinate regional rates of proliferation and regional specification during cardiogenesis. Development 132, 2475–2487.
Cai, X., Nomura-Kitabayashi, A., Cai, W., Yan, J., Christoffels, V.M., Cai, C.L., 2011. Myocardial Tbx20 regulates early atrioventricular canal formation and endocardial epithelial–mesenchymal transition via Bmp2. Dev. Biol. 360, 381–390.
Chen, D., Qiao, Y., Meng, H., Pang, S., Huang, W., Zhang, H., Yan, B., 2013. Genetic analysis of the TBX3 gene promoter in ventricular septal defects. Gene 512, 185–188.
Chen, L., Fulcoli, F.G., Tang, S., Baldini, A., 2009. Tbx1 regulates proliferation and differentiation of multipotent heart progenitors. Circ. Res. 105, 842–851.
Colvee, E., Hurle, J.M., 1983. Malformations of the semilunar valves produced in chick embryos by mechanical interference with cardiogenesis. An experimental approach to the role of hemodynamics in valvular development. Anat. Embryol. (Berl.) 168, 59–71.
de Pater, E., Ciampricotti, M., Priller, F., Veerkamp, J., Strate, I., Smith, K., Lagendijk, A.K., Schilling, T.F., Herzog, W., Abdelilah-Seyfried, S., Hammerschmidt, M., Bakkers, J., 2012. Bmp signaling exerts opposite effects on cardiac differentiation. Circ. Res. 110, 578–587.
Derynck, R., Zhang, Y.E., 2003. Smad-dependent and Smad-independent pathways in TGF-beta family signalling. Nature 425, 577–584.
Dominguez, J.N., Meilhac, S.M., Bland, Y.S., Buckingham, M.E., Brown, N.A., 2012. Asymmetric fate of the posterior part of the second heart field results in unexpected left/right contributions to both poles of the heart. Circ. Res. 111, 1323–1335.
Dupays, L., Kotecha, S., Angst, B., Mohun, T.J., 2009. Tbx2 misexpression impairs deployment of second heart field derived progenitor cells to the arterial pole of the embryonic heart. Dev. Biol. 333, 121–131.
Dyer, L.A., Kirby, M.L., 2009. The role of secondary heart field in cardiac development. Dev. Biol. 336, 137–144.
Ehrlich, M., Gutman, O., Knaus, P., Henis, Y.I., 2012. Oligomeric interactions of TGF-beta and BMP receptors. FEBS Lett. 586, 1885–1896.
Franco, D., Markman, M.M., Wagenaar, G.T., Ya, J., Lamers, W.H., Moorman, A.F., 1999. Myosin light chain 2a and 2v identifies the embryonic outflow tract myocardium in the developing rodent heart. Anat. Rec. 254, 135–146.
Fukuda, T., Scott, G., Komatsu, Y., Araya, R., Kawano, M., Ray, M.K., Yamada, M., Mishina, Y., 2006. Generation of a mouse with conditionally activated signaling through the BMP receptor, ALK2. Genesis 44, 159–167.
Gao, Y., Ma, X.J., Huang, G.Y., Zhang, J., Wang, H.J., Ma, D., Wu, Y., 2012. DNA sequencing of TGFbeta2 in sporadic patients with tetralogy of Fallot. Exp. Ther. Med. 3, 878–880.
Gavrilov, S., Harvey, R.P., Papaioannou, V.E., 2013. Lack of genetic interaction between Tbx20 and Tbx3 in early mouse heart development. PLoS One 8, e70149.
Goracy, I., Safranow, K., Dawid, G., Skonieczna-Zydecka, K., Kaczmarczyk, M., Goracy, J., Loniewska, B., Ciechanowicz, A., 2012. Common genetic variants of the BMP4, BMPR1 A, BMPR1B, and ACVR1 genes, left ventricular mass, and other parameters of the heart in newborns. Genet. Test. Mol. Biomark. 16, 1309–1316.
Guardiola, O., Lafuste, P., Brunelli, S., Iaconis, S., Touvier, T., Mourikis, P., De Bock, K., Lonardo, E., Andolfi, G., Bouche, A., Liguori, G.L., Shen, M.M., Tajbakhsh, S., Cossu, G., Carmeliet, P., Minchiotti, G., 2012. Cripto regulates skeletal muscle regeneration and modulates satellite cell determination by antagonizing myostatin. Proc. Natl. Acad. Sci. USA 109, E3231–3240.
Hogan, B., Beddington, R., Costantini, F., Lacy, E., 1994. Manipulating the Mouse Embryo. A Laboratory Manual. Cold Spring Harbor Laboratory Press, New York
Hutson, M.R., Zeng, X.L., Kim, A.J., Antoon, E., Harward, S., Kirby, M.L., 2010. Arterial pole progenitors interpret opposing FGF/BMP signals to proliferate or differentiate. Development 137, 3001–3011.
Ilagan, R., Abu-Issa, R., Brown, D., Yang, Y.P., Jiao, K., Schwartz, R.J., Klingensmith, J., Meyers, E.N., 2006. Fgf8 is required for anterior heart field development. Development 133, 2435–2445.
Jia, Q., McDill, B.W., Li, S.Z., Deng, C., Chang, C.P., Chen, F., 2007. Smad signaling in the neural crest regulates cardiac outflow tract remodeling through cell autonomous and non-cell autonomous effects. Dev. Biol. 311, 172–184.
Kaartinen, V., Dudas, M., Nagy, A., Sridurongrit, S., Lu, M.M., Epstein, J.A., 2004. Cardiac outflow tract defects in mice lacking ALK2 in neural crest cells. Development 131, 3481–3490.
Kaartinen, V., Nagy, A., 2001. Removal of the floxed neo gene from a conditional knockout allele by the adenoviral Cre recombinase in vivo. Genesis 31, 126–129.
Kirk, E.P., Sunde, M., Costa, M.W., Rankin, S.A., Wolstein, O., Castro, M.L., Butler, T.L., Hyun, C., Guo, G., Otway, R., Mackay, J.P., Waddell, L.B., Cole, A.D., Hayward, C., Keogh, A., Macdonald, P., Griffiths, L., Fatkin, D., Sholler, G.F., Zorn, A.M., Feneley, M.P., Winlaw, D.S., Harvey, R.P., 2007. Mutations in cardiac T-box factor gene TBX20 are associated with diverse cardiac pathologies, including defects of septation and valvulogenesis and cardiomyopathy. Am. J. Hum. Genet. 81, 280–291.
Kishigami, S., Mishina, Y., 2005. BMP signaling and early embryonic patterning. Cytokine Growth Factor Rev. 16, 265–278.
Klaus, A., Saga, Y., Taketo, M.M., Tzahor, E., Birchmeier, W., 2007. Distinct roles of Wnt/beta-catenin and Bmp signaling during early cardiogenesis. Proc. Natl. Acad. Sci. USA 104, 18531–18536.
Liao, J., Aggarwal, V.S., Nowotschin, S., Bondarev, A., Lipner, S., Morrow, B.E., 2008. Identification of downstream genetic pathways of Tbx1 in the second heart field. Dev. Biol. 316, 524–537.
Lindsay, M.E., Schepers, D., Bolar, N.A., Doyle, J.J., Gallo, E., Fert-Bober, J., Kempers, M.J., Fishman, E.K., Chen, Y., Myers, L., Bjeda, D., Oswald, G., Elias, A.F., Levy, H.P., Anderlid, B.M., Yang, M.H., Bongers, E.M., Timmermans, J., Braverman, A.C., Canham, N., Mortier, G.R., Brunner, H.G., Byers, P.H., Van Eyk, J., Van Laer, L., Dietz, H.C., Loeys, B.L., 2012. Loss-of-function mutations in TGFB2 cause a syndromic presentation of thoracic aortic aneurysm. Nat. Genet. 44, 922–927.
Little, S.C., Mullins, M.C., 2009. Bone morphogenetic protein heterodimers assemble heteromeric type I receptor complexes to pattern the dorsoventral axis. Nat. Cell Biol. 11, 637–643.
Macias-Silva, M., Hoodless, P.A., Tang, S.J., Buchwald, M., Wrana, J.L., 1998. Specific activation of Smad1 signaling pathways by the BMP7 type I receptor, ALK2. J. Biol. Chem. 273, 25628–25636.
Manner, J., Seidl, W., Steding, G., 1993. Correlation between the embryonic head flexures and cardiac development. An experimental study in chick embryos. Anat. Embryol. (Berl.) 188, 269–285.
Massague, J., Chen, Y.G., 2000. Controlling TGF-beta signaling. Genes Dev. 14, 627–644.
Mesbah, K., Rana, M.S., Francou, A., van Duijvenboden, K., Papaioannou, V.E., Moorman, A.F., Kelly, R.G., Christoffels, V.M., 2012. Identification of a Tbx1/Tbx2/Tbx3 genetic pathway governing pharyngeal and arterial pole morphogenesis. Hum. Mol. Genet. 21, 1217–1229.
Moorman, A.F., Houweling, A.C., de Boer, P.A., Christoffels, V.M., 2001. Sensitive nonradioactive detection of mRNA in tissue sections: novel application of the whole-mount in situ hybridization protocol. J. Histochem. Cytochem. 49, 1–8.
Onizuka, T., Yuasa, S., Kusumoto, D., Shimoji, K., Egashira, T., Ohno, Y., Kageyama, T., Tanaka, T., Hattori, F., Fujita, J., Ieda, M., Kimura, K., Makino, S., Sano, M., Kudo, A., Fukuda, K., 2012. Wnt2 accelerates cardiac myocyte differentiation from ES-cell derived mesodermal cells via non-canonical pathway. J. Mol. Cell. Cardiol. 52, 650–659.
Pang, S., Liu, Y., Zhao, Z., Huang, W., Chen, D., Yan, B., 2013. Novel and functional sequence variants within the TBX2 gene promoter in ventricular septal defects. Biochimie 95, 1807–1809.
Park, E.J., Ogden, L.A., Talbot, A., Evans, S., Cai, C.L., Black, B.L., Frank, D.U., Moon, A. M., 2006. Required, tissue-specific roles for Fgf8 in outflow tract formation and remodeling. Development 133, 2419–2433.
Ribeiro, I., Kawakami, Y., Buscher, D., Raya, A., Rodriguez-Leon, J., Morita, M., Rodriguez Esteban, C., Izpisua Belmonte, J.C., 2007. Tbx2 and Tbx3 regulate the dynamics of cell proliferation during heart remodeling. PLoS One 2, e398.
Roessler, E., Ouspenskaia, M.V., Karkera, J.D., Velez, J.I., Kantipong, A., Lacbawan, F., Bowers, P., Belmont, J.W., Towbin, J.A., Goldmuntz, E., Feldman, B., Muenke, M., 2008. Reduced NODAL signaling strength via mutation of several pathway members including FOXH1 is linked to human heart defects and holoprosencephaly. Am. J. Hum. Genet. 83, 18–29.
Sakabe, M., Kokubo, H., Nakajima, Y., Saga, Y., 2012. Ectopic retinoic acid signaling affects outflow tract cushion development through suppression of the myocardial Tbx2-Tgfbeta2 pathway. Development 139, 385–395.
Scherptong, R.W., Jongbloed, M.R., Wisse, L.J., Vicente-Steijn, R., Bartelings, M.M., Poelmann, R.E., Schalij, M.J., Gittenberger-De Groot, A.C., 2012. Morphogenesis of outflow tract rotation during cardiac development: the pulmonary push concept. Dev. Dyn. 241, 1413–1422.
Shimmi, O., Umulis, D., Othmer, H., O'Connor, M.B., 2005. Facilitated transport of a Dpp/Scw heterodimer by Sog/Tsg leads to robust patterning of the Drosophila blastoderm embryo. Cell 120, 873–886.
Shore, E.M., Xu, M., Feldman, G.J., Fenstermacher, D.A., Cho, T.J., Choi, I.H., Connor, J. M., Delai, P., Glaser, D.L., LeMerrer, M., Morhart, R., Rogers, J.G., Smith, R., Triffitt, J.T., Urtizberea, J.A., Zasloff, M., Brown, M.A., Kaplan, F.S., 2006. A recurrent mutation in the BMP type I receptor ACVR1 causes inherited and sporadic fibrodysplasia ossificans progressiva. Nat. Genet. 38, 525–527.
Singh, R., Hoogaars, W.M., Barnett, P., Grieskamp, T., Rana, M.S., Buermans, H., Farin, H.F., Petry, M., Heallen, T., Martin, J.F., Moorman, A.F., t Hoen, P.A., Kispert, A., Christoffels, V.M., 2012. Tbx2 and Tbx3 induce atrioventricular myocardial development and endocardial cushion formation. Cell. Mol. Life Sci. 69, 1377–1389.
Singh, R., Horsthuis, T., Farin, H.F., Grieskamp, T., Norden, J., Petry, M., Wakker, V., Moorman, A.F., Christoffels, V.M., Kispert, A., 2009. Tbx20 interacts with smads to confine tbx2 expression to the atrioventricular canal. Circ. Res. 105, 442–452.
Sizarov, A., Lamers, W.H., Mohun, T.J., Brown, N.A., Anderson, R.H., Moorman, A.F., 2012. Three-dimensional and molecular analysis of the arterial pole of the developing human heart. J Anat. 220, 336–349.
Smith, K.A., Joziasse, I.C., Chocron, S., van Dinther, M., Guryev, V., Verhoeven, M.C., Rehmann, H., van der Smagt, J.J., Doevendans, P.A., Cuppen, E., Mulder, B.J., Ten Dijke, P., Bakkers, J., 2009. Dominant-negative ALK2 allele associates with congenital heart defects. Circulation 119, 3062–3069.

Snarr, B.S., Kern, C.B., Wessels, A., 2008. Origin and fate of cardiac mesenchyme. Dev. Dyn. 237, 2804–2819.
Song, L., Fassler, R., Mishina, Y., Jiao, K., Baldwin, H.S., 2007. Essential functions of Alk3 during AV cushion morphogenesis in mouse embryonic hearts. Dev. Biol. 301, 276–286.
Stevens, K.N., Hakonarson, H., Kim, C.E., Doevendans, P.A., Koeleman, B.P., Mital, S., Raue, J., Glessner, J.T., Coles, J.G., Moreno, V., Granger, A., Gruber, S.B., Gruber, P. J., 2010. Common variation in ISL1 confers genetic susceptibility for human congenital heart disease. PLoS One 5, e10855.
Sugi, Y., Ito, N., Szebenyi, G., Myers, K., Fallon, J.F., Mikawa, T., Markwald, R.R., 2003. Fibroblast growth factor (FGF)-4 can induce proliferation of cardiac cushion mesenchymal cells during early valve leaflet formation. Dev. Biol. 258, 252–263.
Takahashi, M., Terasako, Y., Yanagawa, N., Kai, M., Yamagishi, T., Nakajima, Y., 2012. Myocardial progenitors in the pharyngeal regions migrate to distinct cono-truncal regions. Dev. Dyn. 241, 284–293.
Theveniau-Ruissy, M., Dandonneau, M., Mesbah, K., Ghez, O., Mattei, M.G., Miquerol, L., Kelly, R.G., 2008. The del22q11.2 candidate gene Tbx1 controls regional outflow tract identity and coronary artery patterning. Circ. Res. 103, 142–148.
Thomas, P.S., Sridurongrit, S., Ruiz-Lozano, P., Kaartinen, V., 2012. Deficient signaling via Alk2 (Acvr1) leads to bicuspid aortic valve development. PLoS One 7, e35539.
Tian, Y., Yuan, L., Goss, A.M., Wang, T., Yang, J., Lepore, J.J., Zhou, D., Schwartz, R.J., Patel, V., Cohen, E.D., Morrisey, E.E., 2010. Characterization and in vivo pharmacological rescue of a Wnt2-Gata6 pathway required for cardiac inflow tract development. Dev. Cell 18, 275–287.
Tirosh-Finkel, L., Zeisel, A., Brodt-Ivenshitz, M., Shamai, A., Yao, Z., Seger, R., Domany, E., Tzahor, E., 2010. BMP-mediated inhibition of FGF signaling promotes cardiomyocyte differentiation of anterior heart field progenitors. Development 137, 2989–3000.
Verzi, M.P., McCulley, D.J., De Val, S., Dodou, E., Black, B.L., 2005. The right ventricle, outflow tract, and ventricular septum comprise a restricted expression domain within the secondary/anterior heart field. Dev. Biol. 287, 134–145.
Vincent, S.D., Buckingham, M.E., 2010. How to make a heart: the origin and regulation of cardiac progenitor cells. Curr. Top. Dev. Biol. 90, 1–41.
Wang, B., Yan, J., Peng, Z., Wang, J., Liu, S., Xie, X., Ma, X., 2011. Teratocarcinoma-derived growth factor 1 (TDGF1) sequence variants in patients with congenital heart defect. Int. J. Cardiol. 146, 225–227.
Wang, J., Greene, S.B., Bonilla-Claudio, M., Tao, Y., Zhang, J., Bai, Y., Huang, Z., Black, B.L., Wang, F., Martin, J.F., 2010. Bmp signaling regulates myocardial differentiation from cardiac progenitors through a MicroRNA-mediated mechanism. Dev. Cell 19, 903–912.
Wang, J., Sridurongrit, S., Dudas, M., Thomas, P., Nagy, A., Schneider, M.D., Epstein, J.A., Kaartinen, V., 2005. Atrioventricular cushion transformation is mediated by ALK2 in the developing mouse heart. Dev. Biol. 286, 299–310.
Warming, S., Costantino, N., Court, D.L., Jenkins, N.A., Copeland, N.G., 2005. Simple and highly efficient BAC recombineering using galK selection. Nucleic Acids Res. 33, e36.
Watanabe, Y., Zaffran, S., Kuroiwa, A., Higuchi, H., Ogura, T., Harvey, R.P., Kelly, R.G., Buckingham, M., 2012. Fibroblast growth factor 10 gene regulation in the second heart field by Tbx1, Nkx2-5, and Islet1 reveals a genetic switch for down-regulation in the myocardium. Proc. Natl. Acad. Sci. USA 109, 18273–18280.
Xu, H., Morishima, M., Wylie, J.N., Schwartz, R.J., Bruneau, B.G., Lindsay, E.A., Baldini, A., 2004. Tbx1 has a dual role in the morphogenesis of the cardiac outflow tract. Development 131, 3217–3227.
Yang, L., Cai, C.L., Lin, L., Qyang, Y., Chung, C., Monteiro, R.M., Mummery, C.L., Fishman, G.I., Cogen, A., Evans, S., 2006. Isl1Cre reveals a common Bmp pathway in heart and limb development. Development 133, 1575–1585.
Zhang, Z., Huynh, T., Baldini, A., 2006. Mesodermal expression of Tbx1 is necessary and sufficient for pharyngeal arch and cardiac outflow tract development. Development 133, 3587–3595.

Glossary

AoT: Aortic trunk;
AoV: Aortic valve;
AP: Aortico-pulmonary;
AV: Atrioventricular (region);
BMP: Bone morphogenetic protein;
CAT: Common arterial trunk;
cHet: conditional heterozygote;
cKO: conditional knock out;
CNCC: Cardiac neural crest-derived cells;
CHD: Congenital heart disease;
DORV: Double outlet right ventricle;
E9: Embryonic day 9;
EMT: Epithelial-to-mesenchymal transformation;
FGF: Fibroblast growth factor;
ISH: in situ hybridization;
LA: Left atrium;
LV: Left ventricle;
OFT: Outflow tract;
P0: Postnatal, within first 24–h;
PT: Pulmonary trunk;
PV: Pulmonary valve;
RA: Right atrium;
RV: Right ventricle;
RVO: Right ventricular outlet;
SHF: Second heart field;
SmαA: Smooth muscle alpha actin;
VSD: Ventricular septal defect;
WMT: Whole mount (pieces of tissue, not sections).